Open Research Online

The Open University's repository of research publications
and other research outputs

The spread of marine anoxia on the northern Tethys margin during the Paleocene-Eocene Thermal Maximum

Journal Item

How to cite:

Dickson, Alexander J.; Rees-Owen, Rhian L.; März, Christian; Coe, Angela L.; Cohen, Anthony S.; Pancost, Richard D.; Taylor, Kyle and Shcherbinia, Ekaterina (2014). The spread of marine anoxia on the northern Tethys margin during the Paleocene-Eocene Thermal Maximum. Paleoceanography, 29(6) pp. 471–488.

For guidance on citations see FAQs.

© 2014 American Geophysical Union

Version: Version of Record

Link(s) to article on publisher's website:
http://dx.doi.org/doi:10.1002/2014PA002629

Copyright and Moral Rights for the articles on this site are retained by the individual authors and/or other copyright owners. For more information on Open Research Online's data policy on reuse of materials please consult the policies page.

oro.open.ac.uk

AGU PUBLICATIONS

Paleoceanography

RESEARCH ARTICLE
10.1002/2014PA002629

Key Points:
- Reconstruction of northern Peri-Tethys marine redox during the PETM
- Relationship between anoxia, nutrient delivery, and phosphorus recycling
- Main phase of organic carbon burial occurs near the beginning of the PETM

Correspondence to:
A. J. Dickson,
alex.dickson@earth.ox.ac.uk

Citation:
Dickson, A. J., R. L. Rees-Owen, C. März, A. L. Coe, A. S. Cohen, R. D. Pancost, K. Taylor, and E. Shcherbinina (2014), The spread of marine anoxia on the northern Tethys margin during the Paleocene-Eocene Thermal Maximum, *Paleoceanography*, *29*, 471–488, doi:10.1002/2014PA002629.

Received 21 FEB 2014
Accepted 23 APR 2014
Accepted article online 30 APR 2014
Published online 4 JUN 2014

The spread of marine anoxia on the northern Tethys margin during the Paleocene-Eocene Thermal Maximum

Alexander J. Dickson[1,2], Rhian L. Rees-Owen[3,4], Christian März[5], Angela L. Coe[1], Anthony S. Cohen[1], Richard D. Pancost[3], Kyle Taylor[3], and Ekaterina Shcherbinina[6]

[1]Department of Environment, Earth and Ecosystems, Centre for Earth, Planetary, Space and Astronomical Research, Open University, Milton Keynes, UK, [2]Department of Earth Sciences, University of Oxford, Oxford, UK, [3]Organic Geochemistry Unit, The Cabot Institute, School of Chemistry, University of Bristol, Bristol, UK, [4]Now at School of Earth and Environment, University of Leeds, Leeds, UK, [5]School of Civil Engineering and Geoscience, University of Newcastle upon Tyne, Newcastle upon Tyne, UK, [6]Geological Institute, Russian Academy of Sciences, Moscow, Russia

Abstract Records of the paleoenvironmental changes that occurred during the Paleocene-Eocene Thermal Maximum (PETM) are preserved in sedimentary rocks along the margins of the former Tethys Ocean and Peri-Tethys. This paper presents new geochemical data that constrain paleoproductivity, sediment delivery, and seawater redox conditions, from three sites that were located in the Peri-Tethys region. Trace and major element, iron speciation, and biomarker data indicate that water column anoxia was established during episodes when inputs of land-derived higher plant organic carbon and highly weathered detrital clays and silts became relatively higher. Anoxic conditions are likely to have been initially caused by two primary processes: (i) oxygen consumption by high rates of marine productivity, initially stimulated by the rapid delivery of terrestrially derived organic matter and nutrients, and (ii) phosphorus regeneration from seafloor sediments. The role of the latter process requires further investigation before its influence on the spread of deoxygenated seawater during the PETM can be properly discerned. Other oxygen-forcing processes, such as temperature/salinity-driven water column stratification and/or methane oxidation, are considered to have been relatively less important in the study region. Organic carbon enrichments occur only during the initial stages of the PETM as defined by the negative carbon isotope excursions at each site. The lack of observed terminal stage organic carbon enrichment does not support a link between PETM climate recovery and the sequestration of excess atmospheric CO_2 as organic carbon in this region; such a feedback may, however, have been important in the early stages of the PETM.

1. Introduction

The rapid environmental and ecological changes that took place during the Paleocene-Eocene Thermal Maximum (PETM, ~55.9 Ma) [*Westerhold et al.*, 2009; *Charles et al.*, 2011] may hold clues as to how contemporary environmental systems respond to rapid climate changes in the future [*Zachos et al.*, 2008; *McInerney and Wing*, 2011]. One question that can be addressed by studying the PETM is how marine ecosystems and biogeochemical cycles respond to changes in dissolved oxygen concentrations [O_2] in seawater. An increasing number of observations indicate that [O_2] decreased on a global scale during the PETM [*Dickson et al.*, 2012] and at individual locations in shallow marine (<1000 m) [e.g., *Canudo et al.*, 1995; *Speijer et al.*, 1997; *Bolle et al.*, 2000; *Gavrilov et al.*, 2003; *Sluijs et al.*, 2006, 2013; *Soliman*, 2003, *Soliman et al.*, 2011; *Lippert and Zachos*, 2007; *Nicolo et al.*, 2008; *Schulte et al.*, 2011; *Khozyem et al.*, 2013] and at deep marine (>1000 m) [e.g., *Bralower et al.*, 1997; *Thomas*, 1998; *Kaiho et al.*, 2006; *Colisimo et al.*, 2006; *Chun et al.*, 2010] locations. Dissolved [O_2] reflects the balance between the remineralization of sinking organic matter and oxygen ventilation by ocean currents, with preformed [O_2] set by seawater temperature at the air-sea boundary [e.g., *Keeling et al.*, 2010]. In addition, seawater [O_2] during the PETM may also have been affected by the oxidation of methane released from seafloor sediments at the onset of the event [e.g., *Dickens et al.*, 1995, *Dickens*, 2011] and possibly throughout the event [*Zeebe*, 2013]. Thus, observations of lowered [O_2] during the PETM reflect a number of important environmental processes (seawater temperature, ocean circulation, stratification, nutrient cycling, productivity, and methane oxidation); these processes are particularly difficult to disentangle and are likely to have had differing expressions in different oceanographic regions.

©2014. American Geophysical Union. All Rights Reserved.

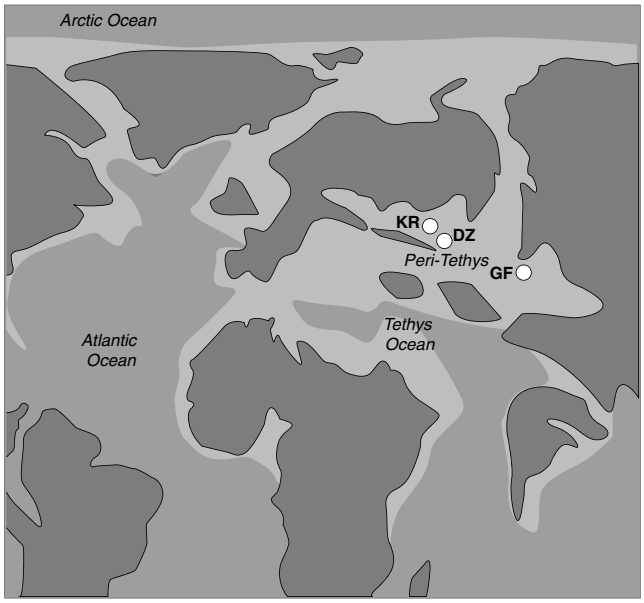

Figure 1. Map of the study locations. KR: Kheu River, DZ: Dzhengutay, GF: Guru-Fatima. Based on paleogeographic reconstructions from www.scotese.com.

Lowered [O_2] often occurs with the enhanced burial of organic carbon (C_{org}) in seafloor sediments. The widespread observation that C_{org} is enriched in marine sediments during brief intervals of the Phanerozoic has led to the idea of "Oceanic Anoxic Events (OAEs)," where low [O_2] conditions favorable to C_{org} preservation expanded dramatically in many oceanographic regions [*Jenkyns*, 2003, 2010]. The PETM has been compared with OAEs on several occasions [e.g., *Cohen et al.*, 2007; *Jenkyns*, 2010], but the magnitude and extent of seawater deoxygenation during the PETM in relation to the earlier events of the Cretaceous and Jurassic is uncertain. Furthermore, it is not clear whether the processes that lowered [O_2] during OAEs were also important for the PETM, when paleogeography, atmospheric pCO_2, and ocean circulation configurations were different [*Jenkyns*, 2010]. The margins of the former Tethys Ocean and northern Peri-Tethys are one of the few regions where C_{org}-enriched sediments accumulated during the PETM in black shale or sapropel horizons analogous to many OAE deposits [e.g., *Gavrilov et al.*, 1997, 2003; *Bolle and Adatte*, 2001; *Speijer and Wagner*, 2002; *Dupuis et al.*, 2003].

Extensive efforts have been made to understand the origin and nature of the Tethyan C_{org}-enriched deposits, and in particular, the unique paleoceanographic conditions that led to their preservation in the geological record. Much of this effort has been directed at locations found on the southern Tethyan margin in present-day North Africa and the Middle East (Figure 1), which form a depth transect extending from upper neritic (<50 m) to lower bathyal (>600 m) water depths [e.g., *Schmitz et al.*, 1996, 1997; *Speijer et al.*, 1997; *Speijer and Schmitz*, 1998; *Speijer and Morsi*, 2002; *Speijer and Wagner*, 2002; *Dupuis et al.*, 2003; *Knox et al.*, 2003; *Soliman*, 2003, *Soliman et al.*, 2011]. At these southern locations, studies have suggested that the C_{org}-rich PETM deposits formed due to a combination of low-[O_2] waters that upwelled along the continental margin, and high rates of marine productivity stimulated by nutrients recycled from deeper water masses and also delivered by high rates of continental erosion and weathering [*Schmitz et al.*, 1997; *Charisi and Schmitz*, 1998; *Speijer and Schmitz*, 1998; *Huber and Sloan*, 2001; *Soliman et al.*, 2011; *Schulte et al.*, 2011; *Stassen et al.*, 2012; *Khozyem et al.*, 2013].

C_{org}-rich deposits on the northern Peri-Tethys margin have been the subject of relatively few publications aimed at investigating the severity of marine deoxygenation during the PETM and about the environmental processes that drove deoxygenation. The climatic response of the Eurasian landmass to PETM environmental change, which may have had an impact on regional deoxygenation, is also poorly known due to a lack of published early Eocene records from central Asia [for example, *Bolle and Adatte*, 2001]. The correlation of C_{org}-rich deposits to global paleoclimate change is also poorly defined in this region, due to the lack of high-resolution carbon isotope records across the PETM interval. Some low-resolution data sets, however, have been produced from shallow-marine exposures in Kazakhstan, Uzbekistan, and southern Russia [*Kodina et al.*, 1995; *Gavrilov et al.*, 1997; *Bolle et al.*, 2000].

Improving the spatial coverage and temporal resolution of environmental proxy data for the PETM from the northern Peri-Tethys region is important, not least because it has been suggested that this region may have acted as a source of low-[O_2] deepwater that subsequently upwelled onto the southern Tethys margin [*Speijer and Wagner*, 2002], or circulated through the Indian and North Atlantic Oceans [e.g., *Pak and Miller*, 1992; *O'Connell et al.*, 1996; *Thomas*, 1998; *Huber and Sloan*, 2001]. An improved record of paleoclimatic and paleoceanographic changes in the northern Peri-Tethys is also important because the enhanced burial of

©2014. American Geophysical Union. All Rights Reserved.

C_{org} in this region has been postulated to act alongside enhanced C burial on other continental margins [e.g., *Speijer and Wagner*, 2002; *John et al.*, 2008] to remove excess CO_2 from the atmosphere [*Gavrilov et al.*, 1997, 2003], ultimately leading to the termination of the PETM.

In this study, multiple geochemical data sets have been produced for three different sites (Guru-Fatima, Kheu River, and Dzhengutay) in the northern Peri-Tethys in order to reconstruct changes in (i) seafloor and water column redox, (ii) marine productivity, and (iii) the delivery of organic and siliciclastic sediments to the study sites from nearby landmasses during the PETM. The results provide insights into the mechanisms that drove regional deoxygenation in the northern Peri-Tethys and new information about the climatic response of nearby landmasses to rapid global climate change.

2. Proxy Approaches

2.1. Redox Proxies

Sedimentary abundances of molybdenum (Mo), rhenium (Re), and manganese (Mn) are strongly redox dependent, and thus reflect $[O_2]$ in seawater at the sediment-water interface and in sediment pore waters [*Emerson and Huested*, 1991; *Crusius et al.*, 1996; *Morford and Emerson*, 1999; *Tribovillard et al.*, 2006]. Manganese exists primarily as Mn(III) and Mn(IV) in oxygenated seawater, within which it forms insoluble Mn-oxyhydroxides. As pore water $[O_2]$ decline, Mn is reduced to soluble Mn(II) that can migrate within the sediment column and reprecipitate as Mn-oxyhydroxides once oxic conditions are reached again [*Tribovillard et al.*, 2006]. Thus, Mn is typically enriched above average shale values in oxygenated sediments located above anoxic to suboxic pore waters or in landlocked anoxic basins where Mn(II) becomes enriched in bottom waters until it reaches Mn(II)-carbonate saturation [e.g., *Pruysers et al.*, 1993; *Higgs et al.*, 1994; *Mangini et al.*, 2001; *Brumsack*, 2006]. Re exists as ReO_4^- in oxic seawater [*Crusius et al.*, 1996]. Under suboxic to anoxic conditions, Re abundances in sediments are typically enriched above average crustal values in sediments [e.g., *Crusius et al.*, 1999; *Morford and Emerson*, 1999; *Calvert and Pederson*, 2007], although the process of removal, whether due to conversion to an insoluble sulfide species or due to coprecipitation with Fe-S-Mo colloidal phases [*Helz et al.*, 2011], is not well understood. Mo typically exists as MoO_4^- in oxygenated seawater and pore waters. At high concentrations of dissolved sulfide, Mo is converted to a tetrathiomolybdate species, MoS_4^{2-}, via a series of intermediate Mo species [*Eriksson and Helz*, 2000; *Tossell*, 2005]. As a particle-reactive sulfide species, Mo is rapidly removed from seawater into marine sediments where it can become greatly enriched above typical crustal abundances of ~1 ppm [*Emerson and Huested*, 1991; *Crusius et al.*, 1996; *Rudnick and Gao*, 2003]. It has been argued that sedimentary enrichments of [Mo] $>$30 ppm indicate euxinic conditions, while enrichments $>$1–30 ppm indicate anoxic, noneuxinic conditions, or a decreased Mo concentrations in the global seawater Mo reservoir [*Scott and Lyons*, 2012].

The proportion of Fe contained within reactive and nonreactive minerals can be used to estimate paleoredox conditions from marine sediments [*Poulton and Canfield*, 2005]. The proportion of highly reactive Fe minerals (Fe_{HR}) among the total Fe pool (Fe_T) does not exceed ~0.38 in most oxic environments [*Raiswell and Canfield*, 1998], while anoxic settings typically display values $>$0.38 due to the input of Fe released from oxygen-depleted shelf sediments (iron shuttle) [*Wijsman et al.*, 2001]. Fe_{HR}/Fe_T ratios from 0.22 to 0.38 are somewhat inconclusive and are termed "possibly anoxic" by *Poulton and Canfield* [2011]. Furthermore, the proportion of pyrite (Fe_{PY}) to Fe_{HR} in marine sediments deposited in euxinic settings is typically $>$0.8 [*Anderson and Raiswell*, 2004], therefore allowing a distinction between Fe-limited (euxinic) and sulfide-limited (ferruginous) anoxic environments based on the amount of reactive Fe that was transformed to pyrite by H_2S [*Poulton and Canfield*, 2011]. Again, there is a range of uncertainty in Fe_{PY}/Fe_{HR} ratios, with values between 0.7 and 0.8 being termed "possibly euxinic" [*Poulton and Canfield*, 2011].

The [lycopane + *n*-C_{35}]/*n*-C_{31} index has been proposed as a paleoredox indicator [*Sinninghe Damste et al.*, 2003]. Although the source organism for lycopane in marine sediments is unknown, it may derive from either methanogenic archaea [e.g., *Brassell et al.*, 1981] or marine phytoplankton [*Wakeham et al.*, 1993; *Sinninghe Damste et al.*, 2003]. Observations of a change in the relative abundance of lycopane and the coeluting C_{35} *n*-alkane versus the C_{31} *n*-alkane in core-top sediments spanning the Arabian and Peruvian upwelling zones [*Schulte et al.*, 1999] led *Sinninghe Damste et al.* [2003] to suggest that the origin of these changes was the greater susceptibility of the precursor lycopene to degradation under oxic conditions compared to *n*-alkanes. Subsequently, lycopane has been used to infer past changes in water column oxygenation in a range of

©2014. American Geophysical Union. All Rights Reserved.

depositional environments [e.g., *Weller and Stein*, 2008; *van Bentum et al.*, 2012], although absolute values of the (lycopane + n-C_{35})/n-C_{31} index are difficult to interpret due to variations in n-alkane dilution and lycopane production [*Sinninghe Damste et al.*, 2003].

Phosphorus (P) is released in preference to carbon during the bacterial remineralization of buried organic matter. In oxygenated pore waters, P can be efficiently trapped by sorption to oxyhydroxide minerals and organic complexes [*Davelaar*, 1993; *Sannigrahi and Ingall*, 2005]. In contrast, the instability of oxyhydroxides under low-[O_2] conditions enhances the flux of reactive P into the overlying water column, while at the same time C_{org} is preferentially preserved, leading to an overall increase in the sedimentary C_{org}/P ratio [*Van Cappellen and Ingall*, 1994; *Algeo and Ingall*, 2007]. This process can lead to a positive feedback of phosphorous regeneration, enhanced primary productivity, reduced [O_2], and further P regeneration during periods of expanded seafloor anoxia [e.g., *Slomp et al.*, 2002; *Mort et al.*, 2007; *Slomp and Van Cappellen*, 2007; *März et al.*, 2008].

2.2. Productivity Proxies

The concentration of low molecular weight (LMW, n-C_{17} + n-C_{19}) n-alkanes, pristane, and phytane have been used to place additional constraints on changes in surface ocean productivity across the PETM at Kheu River. N-alkanes from algal sources are typically LMW (n-C_{15-21}) odd-numbered homologues [*Lytle et al.*, 1979; *Colombo et al.*, 1989; *Rieley et al.*, 1991]. The distribution of algal derived n-alkanes in particular is characterized by a high relative abundance of C_{17} [*Blumer et al.*, 1971; *Giger et al.*, 1980]. Pristane and phytane are thought to originate from the phytyl side chain of chlorophyll a, present in almost all photosynthetic organisms including higher plants, algae, and cyanobacteria [*Rowland*, 1990].

2.3. Continental Weathering and Erosion Proxies

Titanium (Ti) is hosted mainly by high-density Ti-bearing minerals in marine sediments, and tends to concentrate within coarser-grained silt and sand fractions [*Calvert and Pederson*, 2007]. Normalization of Ti to total aluminosilicates can therefore be used as a grain-size proxy because aluminosilicates typically occupy finer-grained clay and silt particle sizes. Aluminum (Al) has been chosen as a proxy for the aluminosilicate fraction because its concentration does not vary greatly between rock types and because it is not strongly affected by biogeochemical processes in the oceans [*Calvert and Pederson*, 2007]. Additionally, Ti/Al ratios in marine sediments can be affected by the changes in source region or in the primary composition of sediments from a single source under extreme weathering conditions that can preferentially remove Al from the host rock [*Young and Nesbitt*, 1998]. To help disentangle these effects, compositional changes of terrestrially derived sediments can also be estimated using the Chemical Index of Alteration (CIA) [*Nesbitt and Young*, 1998]. The CIA is founded on the observation that highly weathered rocks become depleted in the more labile major elements (Ca, K, and Na) during the leaching and alteration of feldspars, leaving a higher relative proportion of less mobile Al. Following a correction for Ca in carbonates, CIA is expressed as

$$\mathrm{CIA} = (\mathrm{Al_2O_3}/(\mathrm{Al_2O_3} + \mathrm{CaO} + \mathrm{K_2O} + \mathrm{Na_2O})) \times 100$$

In addition, the flux of terrestrially derived higher plant biomarkers can be monitored using long-chain n-alkane distributions, and with indices describing the relative abundance of higher plant-derived biomarkers and algal biomarkers. The abundance of terrestrial versus marine-derived organic carbon can be expressed using the odd-over-even preference (OEP) [*Scalan and Smith*, 1970] and carbon-preference (CPI) [*Bray and Evans*, 1961] indices (Figure 4).

3. Methods

3.1. Sampling and Stratigraphy

Three sections (Guru-Fatima, Kheu River, and Dzhengutay) spanning the PETM along the former northern Tethys margin were sampled. The stratigraphies of these sites have been described by *Gavrilov et al.* [1997, 2000, 2003, 2009] and are briefly summarized below and in Figures 2–4.

The Guru-Fatima sedimentary deposits (Figure 2) are composed of grey calcareous marls, overlain by a siltstone with 2.5−20% C_{org}, which grades upward into a grey-brown C_{org} lean marlstone. Evidence for bioturbation is absent during the most C_{org}-enriched marlstone (sapropel), within which horizontal lamination is well developed. At the very top and bottom of the C_{org}-enriched marlstone there is limited

©2014. American Geophysical Union. All Rights Reserved.

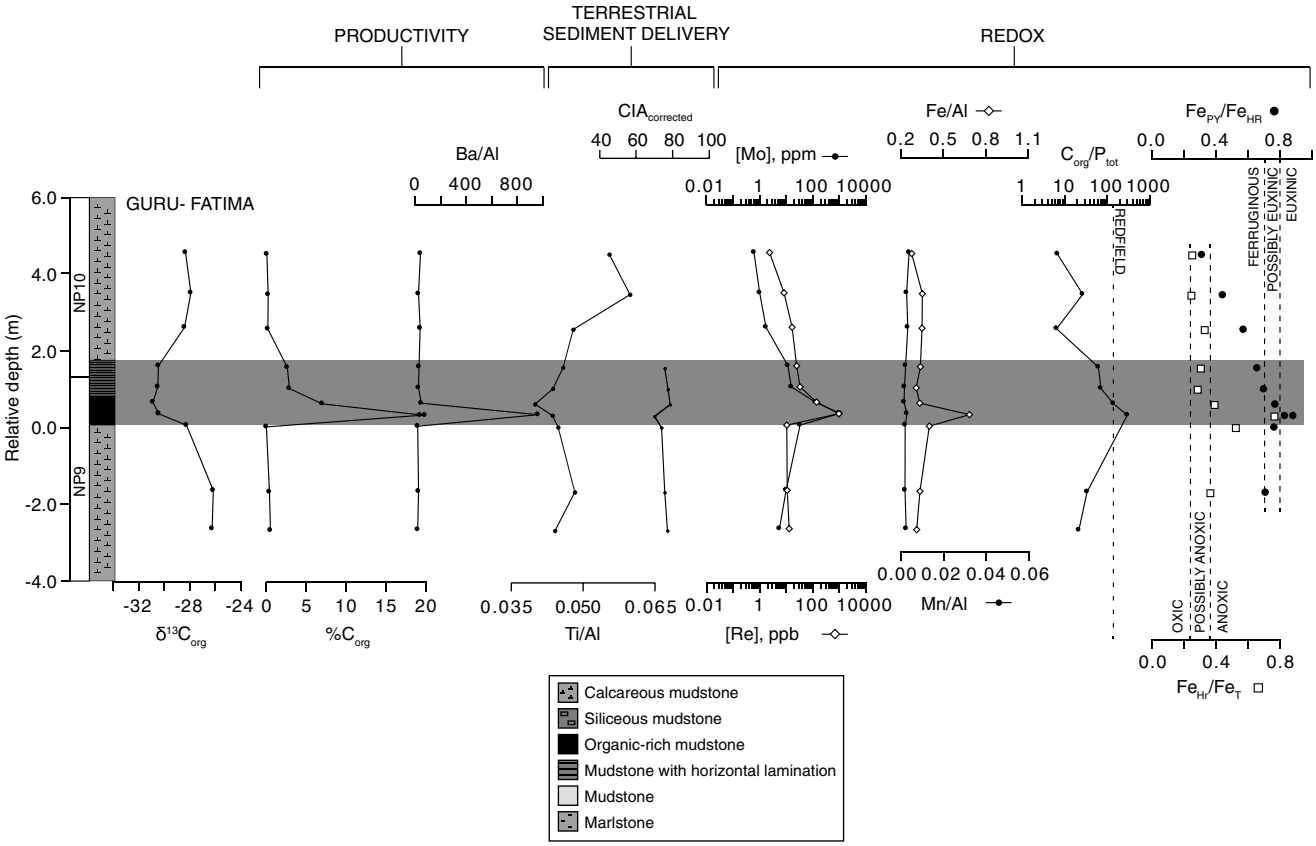

Figure 2. Stratigraphic and geochemical data for Guru-Fatima. Shaded bands denote the interval of enhanced organic carbon abundance (sapropel bed). Dashed lines for the Fe-speciation data show the proposed boundaries between oxic and anoxic, and euxinic and ferruginous sediments [*Raiswell and Canfield*, 1998; *Anderson and Raiswell*, 2004]. Fe_T: total iron, Fe_{HR}: highly reactive iron, Fe_{PY}: pyrite iron.

evidence of millimeter-sized chondrites burrows. Nannofossil biostratigraphy indicates that the NP 9/10 boundary, marked by the first occurrence of *Rhomboaster* spp., is located near the base of the sapropel unit [*Gavrilov et al.*, 2003]. A $\delta^{13}C_{org}$ excursion of −4‰ begins at the base of the sapropel and extends ~1 m above the most C_{org}-enriched unit (Figure 2).

The Kheu River section (Figure 3) is located in the central Northern Caucasus and lies within the Paleogene Nalchik Formation [*Gavrilov and Muzylöv*, 1992; *Gavrilov et al.*, 2000]. The base of the PETM section is composed of greenish-grey calcareous silty claystones, which are overlain by thin grey (~10 cm) organic-lean claystones. Overlying the claystones is ~75 cm of brownish-black silty claystone (sapropel bed), containing varying enrichments of organic carbon (1.5–9% C_{org}). The level of bioturbation varies through the sapropel bed. Millimeter-scale laminations are observed in the basal ~10 cm of the sapropel but are absent further upsection, with evidence for localized chondrites burrows in some intervals. The sapropel bed is overlain by greenish-grey organic-lean shaley siltstones that grade upward into siliciclastic mudstones. Nannofossil biostratigraphy indicates that the sapropel interval falls within NP 9–10, with the NP 9/10 boundary located near the base of the sapropel bed [*Gavrilov et al.*, 2003]. The first occurrence of the dinocyst *Apectodinium augustum* is at the base of the sapropel bed (Figures 2–4). The Kheu River $\delta^{13}C_{org}$ data exhibit a −4.5‰ excursion, beginning at the base of the sapropel and extending ~1.5 m into the overlying siltstones (Figure 3). A >-2‰ excursion in bulk carbonate characterizes the same stratigraphic interval [*Gavrilov et al.*, 2003].

The Dzhengutay section is composed of calcareous mudstones with varying contents of C_{org} (0.1−4%). Nannofossil assemblages indicate that the NP 9/10 boundary falls in the lower part of the sapropel bed [*Gavrilov et al.*, 2009]. The $\delta^{13}C_{org}$ record from this site exhibits a −4‰ excursion (Figure 4). As at Kheu River, the $\delta^{13}C_{org}$ excursion cooccurs with an ~ −1.5‰ $\delta^{13}C$ excursion in bulk carbonates over the same interval

©2014. American Geophysical Union. All Rights Reserved.

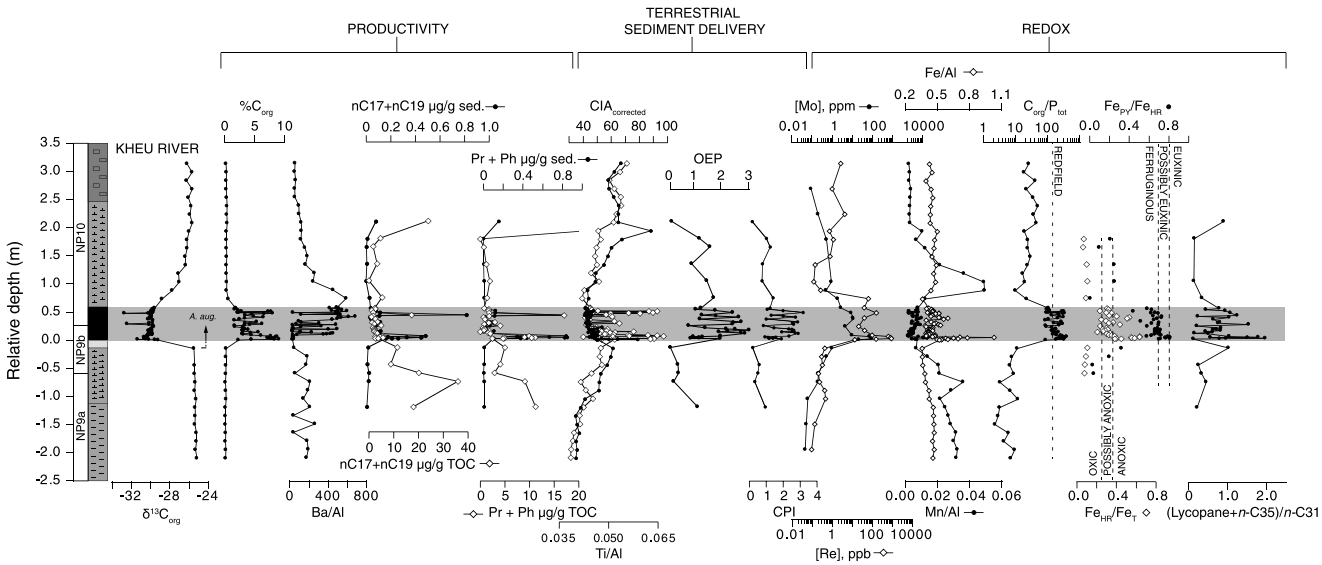

Figure 3. Stratigraphic and geochemical data for Kheu River. *A. aug*: lowest occurrence of *Apectodinium augustum*. OEP index calculated as (C27 + 6*C29 + C31)/(4*C28 + 4*C30) [*Scalan and Smith*, 1970]. CPI calculated as (2*(C25 + C27 + C29 + C31))/(C24 + 2*(C26 + C28 + C30) + C32) [*Bray and Evans*, 1961]. Pr: pristane; Py: phytane. Fe-speciation data labels are the same as for Guru-Fatima.

[*Gavrilov et al.*, 2009]. Evidence for bioturbation is absent in the most C_{org}-enriched interval (Figure 4), but large (several mm diameter) burrows are visible up to 30 cm below the onset of the $\delta^{13}C_{org}$ excursion.

The presence of Midway-type benthic foraminifera species such as *Bulimina midwayensis* and *Anomalinoides* spp., indicates a neritic paleodepth for the three sites [*Stupin and Muzylöv*, 2001; *Radionova et al.*, 2009]. However, elements of Velasco-type fauna such as *Nuttallides truempyi* might also be consistent with a slightly deeper bathyal setting (<1000 m).

Samples from Kheu River and Dzhengutay were obtained from exposures in shallow river cuttings in 2011. The ~75 cm thick Kheu River sapropel bed was sampled in the field as a single block and then subsampled further in the laboratory. Samples for Guru-Fatima were taken from an archived drill core at the Geological Institute of the Russian Academy of Science.

3.2. Major and Trace Elements

The abundances of major element oxides were determined by fusing aliquots of ground sample powders to glass discs with Johnson Matthey Spectroflux® 100A. Analyses were conducted using an ARL 8420+ dual goniometer wavelength dispersive X-ray fluorescence (XRF) spectrometer. Accuracy and precision were monitored with standard reference materials and were both better than ±1%. Abundances of rhenium (Re) and molybdenum [Mo] were determined by isotope dilution. An aliquot of ^{185}Re-enriched and ^{97}Mo and ^{100}Mo-enriched isotope spike was added to 10–100 mg weighed sample powders, which were subsequently digested with a 3:1 mixture of nitric: hydrochloric acid. Re was purified using the liquid-liquid separation technique of *Birck et al.* [1997], and Mo was separated from matrix interferences using the anion column chromatography method of *Pearce et al.* [2009]. Mo and Re were measured using a Thermo-Finnegan Neptune at the Open University. Instrumental mass fractionation for Mo was corrected offline using the ^{97}Mo and ^{100}Mo double spike, and Mo abundances were calculated from the ^{100}Mo/^{95}Mo ratio. Instrumental mass fractionation of Re was corrected by doping each sample solution prior to analysis with an Ir inductively coupled plasma standard solution and normalizing to a ^{193}Ir/^{191}Ir ratio of 1.68299. The external reproducibilities of Re and Mo abundance determinations were monitored using in-house and certified shale (SDO-1) standards and were both better than ±3% (2 standard deviation (SD)).

3.3. Organic Geochemistry

Total carbon (TC) concentrations were determined from 200 mg aliquots of sample powder using a LECO CNS-2000 elemental analyzer at The Open University. Total inorganic carbon (TIC) percentages were

©2014. American Geophysical Union. All Rights Reserved.

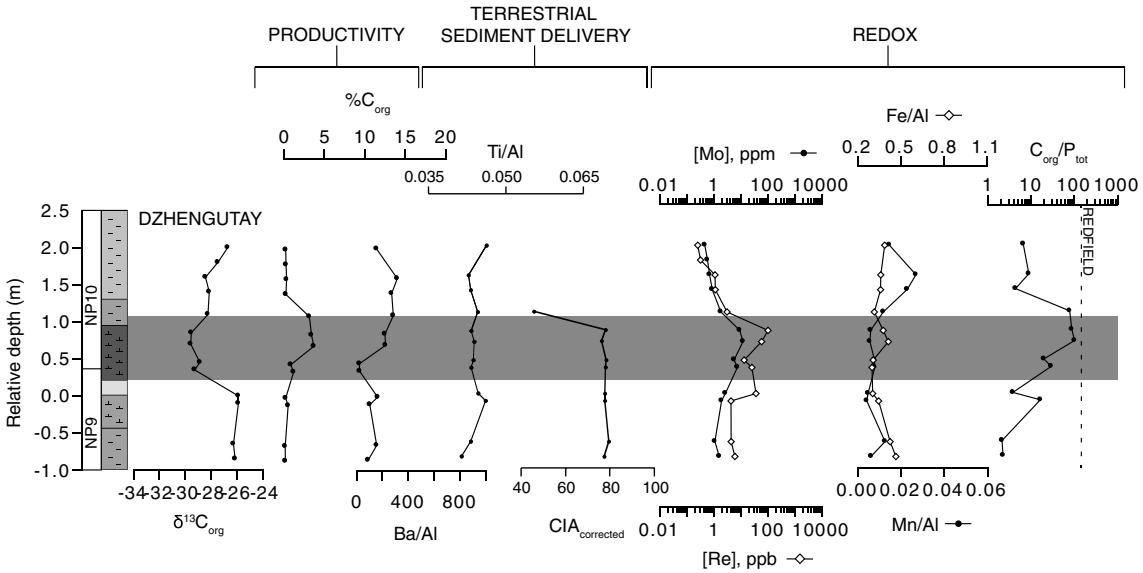

Figure 4. Stratigraphic and geochemical data for Dzhengutay.

determined from a second 500 mg aliquot of sample powder after furnacing for at least 8 h at 450°C. Total organic carbon percentages were calculated by subtracting TIC from TC. For $\delta^{13}C_{org}$ analysis, ground bulk sample powders were decarbonated in sterile glass centrifuge tubes with 0.5N HCl, rinsed in ultrapure water, and oven dried. Decarbonated powders were weighed into tin capsules and analyzed by elemental analysis-isotope ratio mass spectrometry using a Thermo-Finnegan MAT 253. All values are quoted relative to Vienna PeeDee Belemnite. Reproducibility was monitored with repeated analyses of the IAEA CH-6 sucrose standard and was better than ±0.1‰ (1 SD).

Biomarkers were extracted ultrasonically from sample powders using dichloromethane (15 mL × 2), dichloromethane:methanol (15 mL × 2) and methanol (15 mL × 2), combined as the total lipid extract (TLE). Prior to fractionation, sulfur was removed from the TLE using activated copper turnings. The TLEs were separated into two fractions on a silica (40–60 μm, activated; 110°C) column by elution with saturated ammonia in chloroform (7 mL; neutral fraction) and chloroform:acetic acid (100:1; 7 mL; acid fraction). The neutral fraction was further separated on an alumina (Al_2O_3) column by elution with *n*-hexane:dichloromethane (9:1; 5 mL; apolar fraction) and dichloromethane:methanol (1:2; 4 mL; polar fraction). Fatty acid fractions were derivatized with boron trifluoride/methanol (14% w/v; 100 μL; 60°C for 30 min). Prior to analysis, fatty acid and polar fractions were derivatized with *N*,O-bis[trimethylsilyl]trifluoroacetamide and pyridine (1:1; 60 μL; 70°C for 60 min).

Biomarkers from the apolar fraction were quantified using gas chromatography-mass spectrometry (GC-MS) performed on a Thermoquest Finnigan Trace GC interfaced with a Thermoquest Finnigan Trace MS operating with an electron ionization source at 70 eV and scanning over *m/z* ranges of 50 to 850 Daltons. The GC was fitted with a Zebron™ fused silica capillary column (50 m × 0.32 mm ID) coated with a ZB1 stationary phase (100% dimethylpolysiloxane equivalent, 0.12 μm film thickness). The interface was set to 300°C and the ion source at 200°C. Compounds were eluted using He carrier gas. Samples were dissolved in ethyl acetate (10 μL) and injected on column (1 μL) at 70°C. The temperature was increased to 130°C (20°C min^{-1}), then to 300°C (4°C min^{-1}), and held at 300°C for 20 min. Concentrations of biomarkers were calculated from characteristic mass chromatograms and related via a response factor correction to a known amount of internal standard (5α-androstane) quantified on the total ion chromatogram.

3.4. Fe Speciation

A sequential Fe extraction scheme [*Poulton and Canfield*, 2005] was applied to ground sample powders from Kheu River and Guru-Fatima. Briefly, the sequential extraction yields Fe fractions from ~100 mg of sediment extracted with various media, resulting in a differentiation between carbonate-Fe [e.g., siderite; Na-acetate solution], [oxyhydr]oxide-Fe (e.g., hematite, goethite; dithionite solution), and magnetite-Fe [oxalate solution].

©2014. American Geophysical Union. All Rights Reserved.

Iron in the extraction solutions was determined by atomic absorption spectroscopy (Varian 400). The pyrite extraction (~300–700 mg sediment) is based on the quantitative oxidation of pyrite by Cr[III]Cl in a boiling 50% (v/v) HCl solution, the subsequent release of H_2S, its precipitation in a $AgNO_3$ trap, and the quantification of the precipitated AgS. The stoichiometrically calculated FeS_2 fraction is also termed chromium-reducible sulfur or Fe_{PY}. Notably, the acid-volatile sulfide fraction (consisting of Fe sulfides such as greigite and pyrrothite) is negligible in these samples, and pyrite is the only significant Fe sulfide mineral. The sum of all extracted Fe fractions is termed highly reactive Fe (Fe_{HR}), based on the reactivity of these minerals fractions or their precursors with H_2S. The nonextracted Fe, calculated as the difference between total Fe (Fe_T, determined by XRF) and Fe_{HR}, is bound to silicate minerals (e.g., clay minerals, feldspars, pyroxenes, and amphiboles) and is unreactive to H_2S [*Poulton and Canfield*, 2005].

4. Results

4.1. Redox Proxies

4.1.1. Trace and Major Element Enrichments

At all three locations, [Mo] and [Re] become most enriched within the sapropel bed. At Guru-Fatima (Figure 2), [Mo] ranges from 5 to 33 ppm below the sapropel bed and increases to between 126 and >1110 ppm at the same depth as the shift toward more negative $\delta^{13}C_{org}$. Above the sapropel, [Mo] decreases to <1 ppm by +2.55 m. [Re] is elevated above crustal abundances throughout the section and follows the same stratigraphic trend as [Mo], increasing from >10 ppb to >1000 ppb at the base of the sapropel bed, before rapidly declining to <18 ppb by +2.55 m upsection. At Kheu River (Figure 3), [Mo] is <1 ppm below and above the sapropel bed. In the lowest 6 cm of the sapropel, [Mo] increases abruptly to >100 ppm, before decreasing again to between 2 and 12 ppm between 6 and 73 cm depth. [Re] exhibits a near-identical trend, with abundances <0.5 ppb below and above the sapropel and up to ~900 ppb within the basal 6 cm of the sapropel. [Mo] abundances are much lower at Dzhengutay (Figure 4) than at the other two locations, only reaching ~2−4 ppm in the lowest 50 cm of the sapropel bed. [Re] abundances are <5 ppb below and above the sapropel and increase to ≤98 ppb within it.

At Guru-Fatima, Mn/Al is uniformly depleted to average crustal values across the entire section. At Kheu River, Mn/Al decreases progressively upsection from ~0.03 at −2.10 m depth. At the top of the sapropel layer, Mn/Al abruptly rises to ~0.05, at the same stratigraphic level that [Mo] and [Re] rapidly decrease. Mn/Al then falls to average crustal values of ~0.002–0.003 above 208 cm depth, at the same level that $\delta^{13}C_{org}$ returns to preexcursion values. Mn/Al variations at Dzhengutay exhibit a similar stratigraphic trend to Kheu River but with less enrichment of Mn immediately above the sapropel.

4.1.2. Fe Speciation

At Guru-Fatima, Fe_{HR}/Fe_T is >0.38 within the lower 0.5 m of the sapropel. Samples in the lower 0.5 m of the sapropel also display highest Fe/Al ratios, supporting excess Fe input under anoxic conditions (Figure 3). In the upper part of the sapropel, and in overlying sediments, Fe_{HR}/Fe_T is <0.33. Clear evidence for euxinic conditions occurs at +0.3 m, where Fe_{PY}/Fe_{HR} is >0.8 (Figure 3). Fe_{PY}/Fe_{HR} for samples in three other intervals, at ~0 m, ~ + 0.5 m, and ~ +1 m, are >0.7 but <0.8, and thus, the presence of euxinic conditions is more equivocal at these stratigraphic levels. At Kheu River, Fe_{HR}/Fe_T is always <0.1 in deposits above and below the sapropel bed. However, within the sapropel, Fe_{HR}/Fe_T increases above 0.38 in three intervals: between +0 and 0.06 m, at +0.23 m, and from +0.37 to 0.41 m. Fe_{PY}/Fe_{HR} suggests the possible presence of euxinic conditions throughout the sapropel bed (0.7–0.8), whereas values >0.8 are only reached at the base of the sapropel between +0.02 and 0.04 cm.

4.1.3. Lycopane Index [[Lycopane + *n*-C_{35}]/*n*-C_{31}]

The (lycopane + *n*-C_{35})/*n*-C_{31} index varies at Kheu River between 0.13 and 0.45 below and above the sapropel unit (Figure 3). Values are generally higher (>0.5) within the sapropel, with highest values of ~2 in the lowest 6 cm and a second interval of high values >1 occurring between 25 and 50 cm. Values are, however, highly variable, occasionally becoming <0.2.

4.1.4. C_{org}/P Ratios

C_{org}/P ratios at Guru-Fatima, Kheu River, and Dzhengutay (Figures 2–4) are lower above and below the sapropel bed than within it. Minimum values at Kheu River and Dzhengutay (~2) are similar, but maximum values within the sapropel at Kheu (~160) are higher than at Dzhengutay (~100). Values are highest overall at Guru-Fatima, reaching a maximum of ~300 at +0.3 m (Figure 3). Where high-resolution data are available from within the sapropel bed at Kheu River, C_{org}/P ratios fluctuate between ~40 and 160.

©2014. American Geophysical Union. All Rights Reserved.

4.2. Paleoproductivity

A first-order indication of carbon export (paleoproductivity) from the surface ocean is given by C_{org} abundance, which increases markedly during the early part of the PETM at the three study sites. At Guru-Fatima, there is a marked increase in C_{org} from <0.5% to ~20%, at Kheu River C_{org} varies from ~0.1 to ~ 9%, and at Dzhengutay C_{org} varies from <0.1 to ~ 3.5%.

The abundances of $C_{17} + C_{19}$ *n*-alkanes and pristane + phytane can also be used as proxies for total algal inputs to bulk sediment and to indicate the contribution of algal sources to organic detritus. These data are shown for Kheu River in Figure 3. Both sets of biomarker proxies follow near-identical stratigraphic trends that are extremely similar to the bulk C_{org} enrichments when normalized to bulk sediment. Abundances are extremely low (<0.007 μg/g) below the PETM and increase significantly in two intervals (0.00–0.06 m and 0.40–0.50 m) to >0.011 μg/g for pristane + phytane and to >0.012 μg/g for $C_{17} + C_{19}$. When normalized to $\%C_{org}$, both pristane + phytane and $C_{17} + C_{19}$ reach short-term maxima in abundance between 0.00 and 0.06 m, at 0.24 m, and 0.42 m. These increases record times when the algal contribution to total organic carbon increased.

4.3. Terrestrially Derived Sediment Fluxes

4.3.1. Element Ratios

At Guru-Fatima, Ti/Al decreases from ~0.045 to ~0.040 at the onset of the PETM, before rising progressively upsection to a maximum of ~0.06 above 3.45 m. At Kheu River, Ti/Al decreases upsection from values of 0.051 to 0.044 at the base of the sapropel. Minimum values occur at the top of the sapropel bed, before gradually increasing upsection. At Dzhengutay Ti/Al decreases from 0.046 to 0.043 at the onset of the PETM and subsequently increases toward the top of the section. Minimum values of Ti/Al are lower at Dzhengutay and Guru-Fatima than at Kheu River.

CIA values at Dzhengutay and Guru-Fatima are uniformly high (70–80), apart from a single value at Dzhengutay of ~50. The trend in CIA at Kheu River is much more variable. Generally, CIA reflects the overall trend in Ti/Al, from ~30 at the base to ~70 at the top of the section. This upward trend is interrupted across the sapropel by a decline from CIA of ~60 to ~40 (Figure 3). Within the sapropel, CIA increases in short stratigraphic intervals to values of 80–95.

4.3.2. Biomarkers

At Kheu River, OEP and CPI values all increase during the PETM compared to the pre-PETM and post-PETM intervals, indicating a greater input of terrestrial carbon fluxes relative to other sources, including marine algae. The indices are highly variable during the PETM, however, fluctuating between ~0.8 and ~3.2.

5. Discussion

5.1. Influence of Outcrop Weathering on Data Integrity

A key consideration of the present study is whether postdepositional diagenesis and weathering has altered the primary geochemical signals, since these processes may have a measurable effect on the abundance of some trace elements and organic carbon in outcrop sections [e.g., *Peucker-Ehrenbrink and Hannigan*, 2000; *Tribovillard et al.*, 2006; *Georgiev et al.*, 2012]. In the southern Tethyan PETM exposures in Egypt, there is evidence for postdepositional oxidation of pyrite to Fe oxides such as hematite and goethite [*Aubry et al.*, 2007], while Re-Os data from the Paleocene/Eocene Global Standard Stratotype Section and Point at Dababiya Quarry indicate postdepositional remobilization of platinum group elements [*Schmitz et al.*, 2004]. Postdepositional weathering is not considered to compromise the geochemical data presented here because (i) samples were obtained from outcrop sections that were cut back significantly to obtain fresh sample material; (ii) Re-Os evolution plots from all three sections [A. Dickson et al., unpublished data, 2014] indicate very little scatter around identical 55.9 Ma isochrons, indicating minimal remobilization of Re, Os, and potentially other redox sensitive elements; and (iii) Fe speciation might be compromised by weathering, even if total Fe is not affected, due to the conversion of pyrite to Fe oxides (e.g., goethite) and sulfates (e.g., gypsum) in weathered sedimentary deposits. However, no minerals such as gypsum are observed in these deposits, and reactive Fe species follow similar trends at both sites, thus supporting their interpretation as primary depositional signals.

5.2. Redox Variations in the Northern Tethys Ocean

The multiproxy redox data presented in Figure 2 demonstrate that there were pronounced geographic differences in the magnitude of redox change across the early part of the PETM at the three study sites.

©2014. American Geophysical Union. All Rights Reserved.

At Guru-Fatima, Mn/Al ratios are not elevated above average crustal values in the study interval. Since MnO_2 begins to dissolve and act as an electron acceptor below dissolved oxygen concentrations of ~50 μmol/L [*Piper and Calvert*, 2009], the low Mn/Al ratios confirm that sediment pore waters were continually oxygen depleted throughout the study interval. Furthermore, since dissolved Mn^{2+} would tend to accumulate at the suboxic/oxic boundary either at the sediment-water interface, or within sediment pore waters [*Pruysers et al.*, 1993; *Higgs et al.*, 1994; *Mangini et al.*, 2001; *Tribovillard et al.*, 2006], the lack of any significant Mn enrichment at Guru-Fatima suggests that oxygen depletion also extended into bottom waters overlying the sediment-water interface. This inference is consistent with Fe_{HR}/Fe_T values that, while not exceeding the 0.38 threshold for local anoxia [*Poulton and Canfield*, 2011], fall close to it throughout the study interval. It is also consistent with measured C_{org}/P ratios that fall within the range of low $[O_2]$ open ocean shelf settings at the present day [*Algeo and Ingall*, 2007] due to the diffusive loss of P out of the sediments. The new [Mo] data show a similar stratigraphic pattern of enrichment to the lower resolution data of *Gavrilov et al.* [1997] apart from showing an order of magnitude greater enrichment at the base of the sapropel bed. [Re] abundances, measured for the first time from this section, are also significantly enriched above crustal abundances, consistent with the local presence of an oxygen-depleted water mass [*Crusius et al.*, 1996; *Scott and Lyons*, 2012]. The transition to large [Mo] and [Re] enrichments, and Fe_{PY}/Fe_{HR} values >0.8 at the base of the sapropel bed at Guru-Fatima mark a change in bottom water redox toward local anoxia, with some hydrogen sulfide extending into the water column [*Emerson and Huested*, 1991; *Crusius et al.*, 1996; *Poulton and Canfield*, 2011; *Scott and Lyons*, 2012]. The presence of euxinic conditions is supported by the presence of isorenieratene-derived diaryl isoprenoids in the stratigraphically equivalent sapropel bed at the Kurpai section, which is located close to Guru-Fatima [*Kodina et al.*, 1995; *Gavrilov et al.*, 1997].

In contrast to the stable deoxygenated bottom waters at Guru-Fatima, the local redox state was more variable through time at Dzhengutay and Kheu River. At these two locations, Mn/Al ratios are more variable and in particular exhibit a pronounced level of enrichment above the sapropel bed. These geochemical patterns are typical of Mediterranean sapropels, where they indicate the presence of a sharp redoxcline separating low-$[O_2]$ sediment pore waters from well-oxygenated bottom waters, with upward migration of the Mn-enriched layer as sedimentation progresses throughout deposition of the sapropel bed [e.g., *Pruysers et al.*, 1993; *Higgs et al.*, 1994; *Mangini et al.*, 2001]. Accordingly, [Mo] enrichments never exceed ~4 ppm at Dzhengutay or ~12 ppm at Kheu River [apart from in the lowermost 6 cm of the sapropel bed in the latter section]. This level of enrichment is consistent with the fixation of Mo as MoS_x in sulfidic pore waters, followed by dissolution and readsorption to Mn- and Fe-oxyhydroxides during periods when the redoxcline fluctuated across the sediment-water interface [*Reitz et al.*, 2007; *Lyons and Severmann*, 2006]. Fluctuation of the chemocline is also indicated by (i) variable, but overall higher lycopane indices within the sapropel bed, which indicates the temporary extension of the chemocline into the overlying water column; (ii) fluctuations in Fe_{HR}/Fe_T that correspond to variations in the lycopane index; and (iii) the cooccurrence of sedimentary laminations and bioturbation within the sapropel bed (Figure 2). The overall picture for Kheu River is of an anoxic setting with episodic bottom water ventilation that allowed $[O_2]$ to penetrate into sediment pore waters and alter primary geochemical signatures.

A similar scenario has been interpreted from correlative Tethyan sections at shallow (Wadi Nukhl, Egypt) and upper bathyal (Torangli, Turkmenistan) depths by *Speijer et al.* [1997]. At these locations, the depositional sequence across the PETM sapropel bed is marked by the replacement of a diverse benthic community by low-diversity opportunistic taxa that may have colonized the seafloor during very brief intervals when low-$[O_2]$ conditions were ameliorated by bottom water reoxidation.

The Kheu River and Dzhengutay redox data sets exhibit many similarities, but there are also some key differences. At Dzhengutay, Mn/Al ratios are close to average crustal values below the onset of the PETM, while they are significantly elevated above average crustal values at Kheu River. Similarly, [Re] enrichments below the PETM at Dzhengutay are also elevated, albeit by a small amount, while no such enrichment can be seen at Kheu River. Together, these differences suggest that pore waters at Dzhengutay were also intermittently suboxic before the deposition of the sapropel bed, similar to the more severe pre-PETM $[O_2]$ depletion seen at Guru-Fatima further to the east.

The multiproxy redox data presented in Figures 2–4 are consistent with the continual presence of $[O_2]$-depleted bottom waters at shallow depths in the northeastern Peri-Tethys during the latest Paleocene and early Eocene.

©2014. American Geophysical Union. All Rights Reserved.

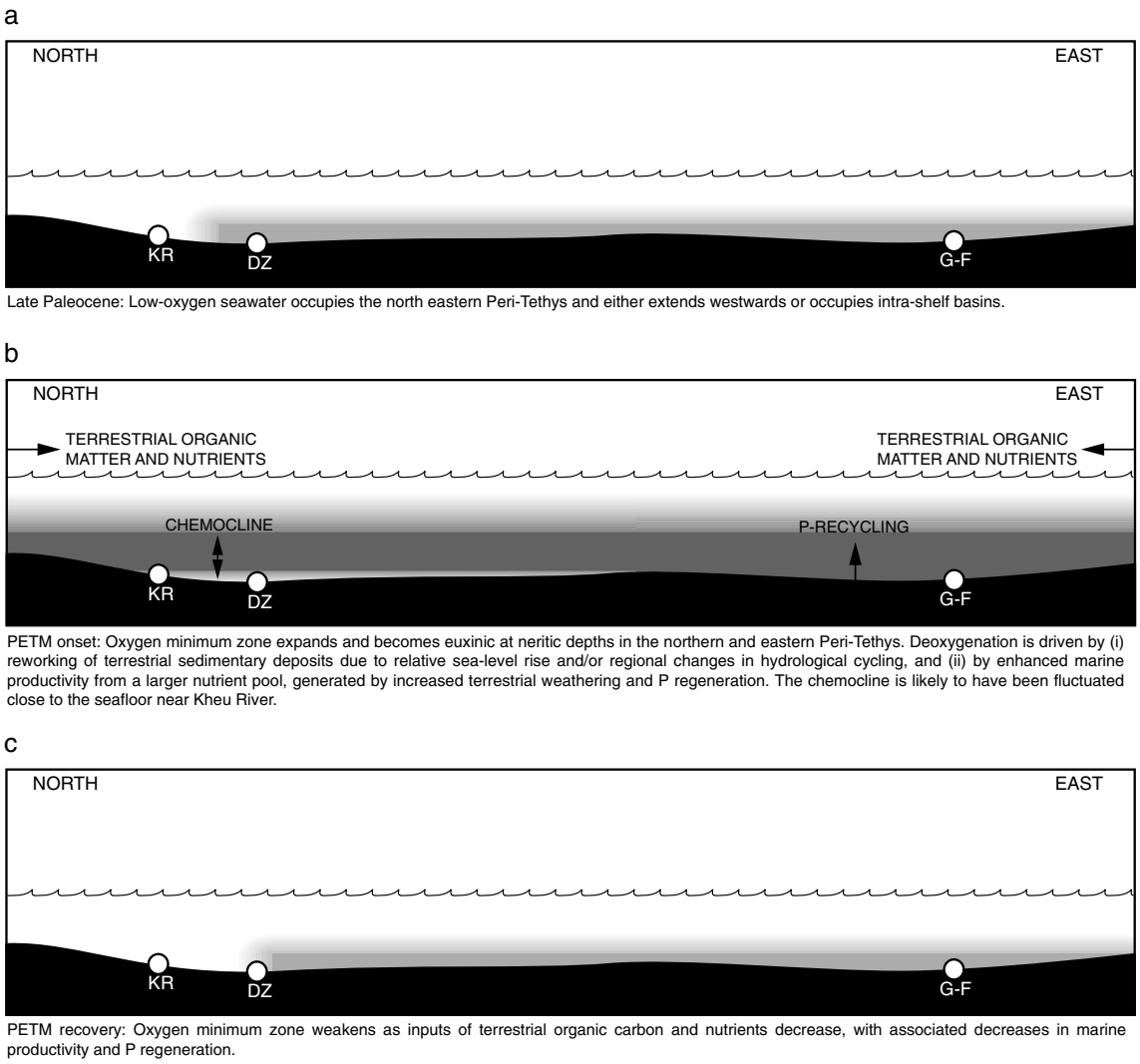

Figure 5. Schematic representation of paleoceanographic changes in the northern Peri-Tethys (a) before, (b) during, and (c) after the PETM. Shaded areas indicate areas of low-oxygen seawater. In Figure 5b, deoxygenated waters intensify in response to oxygen consumption during the remineralization of higher fluxes of organic carbon (terrestrial and marine) near the seafloor. Redox indicators for Kheu River suggest that localized anoxia did not continually affect the seafloor but probably fluctuated with occasional reoxidation events and migration of the redoxcline across the seawater-sediment interface.

These low-[O_2] conditions extended westward, where they influenced the bottom water environment at Dzhengutay but were less profoundly felt at Kheu River. At the onset of the PETM, low-[O_2] conditions intensified at all sites, driving bottom waters to anoxia at Kheu River. At the start of the recovery phase toward the end of the PETM, marked by a return to preexcursion $\delta^{13}C_{org}$ values at each site, severe marine deoxygenation in the northern Peri-Tethys abruptly ended, with water masses near to Kheu River becoming well oxygenated once again, and seawater in the eastern Peri-Tethys at Guru-Fatima becoming suboxic once again (Figure 5). The exact point in the sections at which low-[O_2] conditions abated is difficult to identify, however, due to the possible impact of postdepositional oxidation into organic-rich near-surface sediments [e.g., *Pruysers et al.*, 1993; *Higgs et al.*, 1994].

A similar pattern of deoxygenation has also been documented by *Bolle et al.* [2000] at the Aktumsuk and Kautarkapy sections in Kazakhstan. These authors also found lycopane in the Aktumsuk sapropel bed, which is stratigraphically equivalent to the sections studied here. Taken together, the evidence presented in this study and by *Bolle et al.* [2000] suggests that a layer of [O_2]-depleted water was present at shallow depths in the eastern Peri-Tethys during the late Paleocene and intensified and spread westward in response to the environmental changes that took place during the PETM.

©2014. American Geophysical Union. All Rights Reserved.

5.2.1. Mechanisms of Deoxygenation in the Northern Peri-Tethys

5.2.1.1. Influence of Marine Productivity on Redox

Organic carbon contents increase by 50-, 35-, and 15- fold over preexcursion contents at Kheu River, Guru-Fatima, and Dzhengutay, respectively. Such large increases in C_{org} are unlikely to have occurred only due to enhanced preservation of organic carbon, particularly since low-[O_2] conditions at Guru-Fatima were stable throughout sapropel deposition. Thus, in line with studies from other time intervals [e.g., *Passier et al.*, 1999; *Kuypers et al.*, 2002] preservation alone cannot explain such elevated C_{org} abundances and enhanced primary production must also be invoked. High marine organic carbon fluxes in response to increased productivity are supported by the high abundances of Pr + Ph and $C_{17} + C_{19}$ *n*-alkanes at Kheu River, particularly in the lowermost ~10 cm of the sapropel bed where independent redox indicators show that deoxygenation was most pronounced. Elevated marine productivity will have had a strong influence on the consumption of dissolved oxygen, as indicated by the correlation between highest fluxes of algal biomarkers and the presence of anoxic/euxinic conditions in the sapropel bed at Kheu River.

There are several potential sources of nutrients into the northern Tethys Ocean that could have caused higher rates of organic carbon production. The first of these is the weathering and/or erosion of continental organic matter and lithogenic sediment and its transport and deposition along the continental shelf and upper slope. The CPI and OEP indices at Kheu River both show an increase in the abundance of higher plant-derived biomarkers recorded during deposition of the sapropel bed. This influx of higher plant organic carbon can be correlated to pulses of highly weathered lithogenic material recorded by large increases in CIA values and (at the base of the sapropel bed) by a spike in Ti/Al [e.g., *Young and Nesbitt*, 1998]. Taken together, these lines of evidence point toward the erosion of terrestrial organic carbon, possibly from weathered soil profiles, followed by transport out onto the continental shelf and slope. The additional nutrient fluxes could have stimulated primary productivity in the northern Tethys water column, further consuming available oxygen and creating anoxic seafloor conditions.

The importance of continental erosion and weathering on the availability of nutrients is not a phenomenon confined to the northern Peri-Tethys. There are numerous examples from locations such as New Zealand [*Crouch et al.*, 2003; *Hollis et al.*, 2005; *Nicolo et al.*, 2008], the New Jersey shelf [*Gibbs et al.*, 2006; *John et al.*, 2008; *Sluijs and Brinkhuis*, 2009], the Arctic Ocean [*Sluijs et al.*, 2006; *Stein et al.*, 2006; *Harding et al.*, 2011], the southern Tethys Ocean [*Speijer and Schmitz*, 1998; *Soliman et al.*, 2011; *Schulte et al.*, 2011], and Tanzania [*Handley et al.*, 2012] where terrestrial sediment accumulation rates and nutrient availability increased during the PETM. Enhanced rates of continental weathering are likely to have been a global feature of the PETM [*Ravizza et al.*, 2001]. Some studies have inferred geographical changes in the hydrological cycle during the PETM [e.g., *Pagani et al.*, 2006], whereas others have stressed the role of enhanced seasonality in moisture delivery (i.e., more frequent, intense rainy seasons) in creating conditions favorable for rapidly eroding large volumes of sediment onto continental margins [*Schmitz and Pujalte*, 2007; *Handley et al.*, 2012]. Furthermore, the delivery of terrestrially derived sediments and nutrients could have been controlled by a global transgressive event at the start of the PETM [*Sluijs et al.*, 2008] that also influenced the Tethys Ocean margin [*Gavrilov et al.*, 1997, 2003; *Speijer and Morsi*, 2002]. Sea level rise is likely to have been an important control on nutrient delivery to the northern Peri-Tethys, since sea level rise would have flooded large areas of a broad continental shelf [*Gavrilov et al.*, 1997, 2003]. A similar sea level mechanism for remobilizing terrestrial nutrients during OAE-2 (Cenomanian-Turonian boundary event) has recently been proposed by *Gavrilov et al.* [2013].

A second possible source of nutrients into the study region during the PETM is from the recycling of P from sediments during the breakdown of organic matter under low-[O_2] bottom water conditions. In this scenario, the development of bottom water deoxygenation would increase the regeneration of organic P, which would thus act as a positive feedback to sustain deoxygenated conditions by fueling further organic carbon production [e.g., *Algeo and Ingall*, 2007; *Mort et al.*, 2007]. The C_{org}/P molar ratio becomes higher during the sapropel interval of all three sites studied here (Figures 2–4). Assuming a typical Redfield ratio for marine phytoplankton of ~106, C_{org}/P ratios during the sapropel beds of >150 at Kheu River and >300 at Guru-Fatima might indicate a preferential release of P under locally anoxic bottom waters. At Dzhengutay, C_{org}/P ratios only reach ~100, suggesting that while P regeneration may have taken place, the primary control is likely to have been better preservation of organic matter on the seafloor. A confounding factor on interpreting the C_{org}/P ratios at the three Tethys sites is that organic matter from terrestrial plants and soils typically have higher C_{org}/P

©2014. American Geophysical Union. All Rights Reserved.

ratios than marine algae [*Cleveland and Liptzin*, 2007]. An increase in higher plant organic C fluxes, as indicated by the CPI and OEP indexes at Kheu River, is therefore another means of raising C_{org}/P ratios within the sapropel bed. Assuming an average C_{org}/P ratio for soil of ~190 [*Cleveland and Liptzin*, 2007] and no differential preservation in different organic matter types, the high C_{org}/P ratios within the sapropel bed at Kheu River could be explained by a ~55% contribution of land-derived organic matter, while those at Dzhengutay could be explained by a ~5% contribution. The C_{org}/P ratio of ~300 at Guru-Fatima is difficult to explain even by a total dominance of land-derived organic matter, and thus is the only site where P regeneration can be reliably assumed. In summary, P regeneration is likely to have played a role in stimulating primary production and driving regional deoxygenation along the northern Tethys margin, but its influence is difficult to disentangle from the available C_{org}/P data. The suggestion that P regeneration is important at a global scale for the PETM [*Sluijs et al.*, 2013] may be correct but cannot be assumed on the basis of limited existing data.

5.2.1.2. Influence of Surface Water Temperature and Salinity on Redox

Temperature and salinity could have had a marked effect on seawater deoxygenation in the study region by altering the air-sea exchange of [O_2] and by controlling the degree of surface water stratification, and hence subsurface ventilation. However, no proxy reconstructions of these parameters are currently available from this region. *Winguth et al.* [2010] modeled either an increase in northern Tethys surface salinity of 0.5–9 practical salinity unit during the PETM or a slight decrease in salinity depending on the direction of freshwater export from the Arctic Ocean. An increase in surface salinity has also been suggested by *Cope and Winguth* [2011], who attributed this effect to a deepening of the mixed layer due to reduced surface buoyancy. Different versions of the Goddard Institute for Space Studies general circulation model produce qualitatively similar increases in subtropical salinity centered on the northern Tethys [*O'Connell et al.*, 1996; *Roberts et al.*, 2009], although these increases are quantitatively smaller than those produced by *Cope and Winguth* [2011]. The modeling data suggest that the [O_2]-depleted and nutrient-rich waters inferred to have existed in the northern Peri-Tethys could have been exported to the wider region within a high-salinity water mass, thus influencing the spread of deoxygenated waters along the southern Tethyan margin, and to an extent in the open Indian and Southern Oceans. This argument is partially supported by the global distribution of faunal, sedimentological, and geochemical indicators of low-[O_2] conditions during the PETM [*Thomas*, 1998; *Chun et al.*, 2010] and by carbon isotope indicators of water mass aging in the Indian Ocean [*Seto*, 1995]. However, these arguments still need to be verified by proxy data reconstructions in this region.

It has been suggested that anoxia on the southern Tethys margin during the PETM was partly controlled by regional upwelling, which drove high levels of primary productivity [e.g., *Schmitz et al.*, 1997; *Speijer et al.*, 1997; *Charisi and Schmitz*, 1998; *Speijer and Schmitz*, 1998]. In contrast, upwelling along the northern Peri-Tethys margin is difficult to envisage due to modeled high-salinity and temperature conditions. Furthermore, wind directions along the northern Tethys margin were unlikely to have favored Ekman divergence [*O'Connell et al.*, 1996; *Huber and Sloan*, 2001], plus the broad, shallow paleogeography of the northern Peri-Tethys was not suitably configured to allow nutrient-rich waters from the open Tethys Ocean to penetrate below the surface mixed layer [*Gavrilov et al.*, 1997]. The apparent synchrony in the timing of anoxia in both the northern Peri-Tethys and the southern Tethys Ocean regions, therefore, must be due to synchronous changes in environmental conditions over the entire region or by a direct teleconnection between the two regions. One possible teleconnection might be the export and advection of low-[O_2] water from the northern Peri-Tethys onto the southern Tethys Ocean continental shelf [*Speijer et al.*, 1996].

5.2.1.3. Influence of Methane Release on Redox

The strongest evidence for a possible role for methane oxidation as a cause of regional deoxygenation is the temporal coincidence between the timing of the most severe phase of anoxia in the northern Tethys Ocean (as indicated by Fe speciation, [Mo] and [Re] abundances and lycopane index values at Kheu River and Guru-Fatima) and the onset of the carbon isotope excursion (CIE). A similar coincidence in the timing of suboxic conditions and the onset of the CIE was noted for the New Zealand margin by *Nicolo et al.* [2010]. Deoxygenation in the New Zealand margin was partly attributed to the oxidation of methane, given the absence of evidence of additional mechanisms for consuming oxygen. Assuming a release of ~3000 pg of methane-derived C during the PETM [*Zeebe et al.*, 2009], and a mass of oxygen in the oceans and atmosphere of $\sim 3.8 \times 10^{19}$ mol [*Duursma and Boisson*, 1994], the oxidation of methane to CO_2 would have consumed $<$2% of available free oxygen. If a further assumption is made that most oxygen consumption would have occurred in the atmosphere (which fits with observations that the CIE is more pronounced in shallower PETM

©2014. American Geophysical Union. All Rights Reserved.

sites and in planktonic foraminifera than benthic foraminifera [*Zachos et al.*, 2007]), the oxidation of methane would have had the effect of lowering seawater [O_2] from its global mean of ~2 μmol/L by only a small amount. Furthermore, the warm, relatively shallow Peri-Tethys locations studied here are unlikely regions for extensive methane hydrate formation. Even if hydrates were forming at deeper Tethyan locations, the absence of upwelling for the study region implies that it is unlikely that this methane would have affected the ventilation of water masses overlying the study sites.

In summary, while the effects of methane oxidation on [O_2] are not likely to have been globally uniform, and cannot be entirely ruled out for the northern Tethys Ocean, the wealth of additional proxy data presented here points to the dominant role of organic C remineralization leading to oxygen depletion and water column anoxia in the study region.

6. Comparison of the PETM to Mesozoic OAEs

The scenario outlined for the northern Tethys during the PETM bears some similarities to those described for the OAEs that occurred during the Cretaceous and Jurassic eras [*Jenkyns*, 2003]. It has been proposed that marine productivity became significantly elevated during OAEs due to higher terrestrially derived nutrient fluxes [e.g., *Cohen et al.*, 2004, 2007; *Adams et al.*, 2010; *Monterio et al.*, 2012; *Gavrilov et al.*, 2013]. During OAE-2 (the Cenomanian-Turonian event) the most severely reducing marine conditions, with euxinic waters extending upward into the euphotic zone, have been found within the proto-North Atlantic basin, where continental alignment created a nutrient trap with limited deepwater renewal across shallow bordering seaways [e.g., *Kuypers et al.*, 2002; *Pancost et al.*, 2004; *Jenkyns*, 2010; *Jimenez Berrocoso et al.*, 2010]. Conversely, in settings such as Exmouth Plateau (Indian Ocean) and Demerara Rise (central Atlantic Ocean), anoxic conditions intensified mainly within oxygen minimum zones that impinged on continental margins, presumably due to proximity to weathered nutrients [e.g., *Thurow et al.*, 1992; *Friedrich et al.*, 2006]. Anoxia was punctuated by intervals of episodic deepwater ventilation at these locations, although the exact cause of these ventilation episodes is currently not well understood [e.g., *Friedrich*, 2010].

In direct comparison with the proto-North Atlantic Ocean during OAE-2, the hydrographically restricted Arctic Ocean likely acted as a nutrient trap during the PETM, with euxinic waters extending upward into the euphotic zone in response to greater fluxes of nutrients weathered from neighboring landmasses [*Sluijs et al.*, 2006; *Weller and Stein*, 2008; *Dickson et al.*, 2012]. Furthermore, in the northern Peri-Tethys, anoxia seems to have developed during the PETM in a fashion akin to Exmouth Plateau and Demerara Rise during OAE-2, with the intensification of a preexisting low-[O_2] water mass, the development of anoxic/euxinic seafloor conditions, and the punctuation of these extreme conditions by intervals of episodic bottom water ventilation. In summary, the PETM may have been affected by similar environmental conditions that resulted in the formation of OAEs but was possibly preconditioned toward less extensive global anoxia by a different paleogeography. In this sense it may be considered as an incipient OAE [*Cohen et al.*, 2007].

7. Conclusions

New geochemical data from three sites spanning the PETM document the expansion of anoxic water masses across a wide region of the northern and eastern Peri-Tethys and provide evidence for what caused deoxygenation in this region. The development of anoxia appears to have been a response primarily to the stimulation of marine productivity by an increase in nutrient availability. The increase in nutrients was likely to have been caused by both terrestrial weathering and the regeneration of buried P from marine sediments along the Peri-Tethys margin. However, evidence for the latter process, for which those data presented here are the first for the PETM, is still sparse.

The most significant organic carbon enrichment in the northern Peri-Tethys occurred during the first part of the PETM. Although some organic carbon may have been lost from the uppermost parts of the PETM sections studied here by postdepositional "burn down," these results suggest that carbon burial was not widespread in the region during the recovery phase of the PETM. For that reason, organic carbon burial in the northern Peri-Tethys is unlikely to have played a role in sequestering excess CO_2 from the atmosphere during the terminal phase of the PETM, although carbon burial on other continental margins could have had an effect on CO_2 drawdown [e.g., *John et al.*, 2008].

©2014. American Geophysical Union. All Rights Reserved.

Acknowledgments
We wish to thank Jon Watson and Manuela Fehr for laboratory assistance. A.J.D., A.S.C., and A.L.C. were supported by NERC grant NE/F021313/1. C.M. was funded by the Deutsche Forschungsgemeinschaft (grant MA 4791-2/1). R.D.P. was supported by a Royal Society Wolfson Research Merit Award. Data in this paper may be obtained from the first author or from www.pangaea.de.

References

Adams, D. D., M. T. Hurtgen, and B. B. Sageman (2010), Volcanic triggering of a biogeochemical cascade during Oceanic Anoxic Event 2, *Nat. Geosci.*, *3*, 201–204.

Algeo, T. J., and E. Ingall (2007), Sedimentary C_{org}:P ratios, paleocean ventilation, and Panerozoic atmospheric pO_2, *Palaeogeogr. Palaeoclimatol. Palaeoecol.*, *256*, 130–155.

Anderson, T. F., and R. Raiswell (2004), Sources and mechanisms for the enrichment of highly reactive iron in euxinic Black Sea sediments, *Am. J. Sci.*, *304*, 203–233.

Aubry, M.-P., K. Ouda, C. Dupuis, W. A. Berggren, J. A. van Couvering, and members of the Working Group on the Paleocene/Eocene boundary (2007), The Global Standard Stratotype-Section and Point (GSSP) for the base of the Eocene Series in the Dababiya section (Egypt), *Episodes*, *30*, 271–286.

Birck, J. L., M. Roy Barman, and F. Capmas (1997), Re-Os isotopic measurements at the femtomole level in natural samples, *Geostand. Newslett.*, *20*, 19–27.

Blumer, M., R. R. Guillard, and T. Chase (1971), Hydrocarbons of marine phytoplankton, *Mar. Biol.*, *8*, 183.

Bolle, M.-P., and T. Adatte (2001), Palaeocene-early Eocene climatic evolution in the Tethyan realm: Clay mineral evidence, *Clay Miner.*, *36*, 249–261.

Bolle, M. P., A. Pardo, K.-U. Hinrichs, T. Adatte, K. von Salis, S. Burns, G. Keller, and N. Muzylev (2000), The Paleocene-Eocene transition in the marginal northeastern Tethys [Kazakhstan and Uzbekistan], *Int. J. Earth Sci.*, *89*, 390–414.

Bralower, T. J., D. J. Thomas, J. C. Zachos, M. M. Hirschmann, U. Röhl, H. Sigurdsson, E. Thomas, and D. L. Whitney (1997), High-resolution records of the late Paleocene thermal maximum and circum-Caribbean volcanism: Is there a causal link?, *Geology*, *25*, 963–966.

Brassell, S. C., A. M. K. Wardroper, I. D. Thomson, J. R. Maxwell, and G. Eglinton (1981), Specific acyclic isoprenoids as biological markers of methanogenic bacteria in marine sediments, *Nature*, *290*, 693–696.

Bray, E. E., and E. D. Evans (1961), Distribution of n-paraffins as a clue to recognition of source beds, *Geochim. Cosmochim. Acta*, *22*, 2–15.

Brumsack, H.-J. (2006), The trace metal content of recent organic carbon-rich sediments: Implications for Cretaceous black shale formation, *Palaeogeogr. Palaeoclimatol. Palaeoecol.*, *232*, 344–361.

Calvert, S. E., and T. F. Pederson (2007), Elemental proxies for palaeoclimatic and palaeoceanographic variability in marine sediments: Interpretation and application, *Dev. Mar. Geol.*, *1*, 567–644.

Canudo, J. I., G. Keller, E. Molina, and N. Ortiz (1995), Planktic foraminiferal turnover and 13C isotopes across the Paleocene-Eocene transition at Caravaca and Zumaya, Spain, *Palaeogeogr., Palaeoclimatol., Palaeoecol.*, *114*, 75–100.

Charisi, S. D., and B. Schmitz (1998), Paleocene to early Eocene paleoceanography of the Middle East: The $\delta^{13}C$ and $\delta^{18}O$ isotopes from foraminiferal calcite, *Paleoceanography*, *13*, 106–118, doi:10.1029/97PA02585.

Charles, A. J., D. J. Condon, I. C. Harding, H. Pälike, J. E. A. Marshall, Y. Cui, L. Kump, and I. W. Croudace (2011), Constraints on the numerical age of the Paleocene-Eocene boundary, *Geochem. Geophys. Geosyst.*, *12*, Q0AA17, doi:10.1029/2010GC003426.

Chun, C. O. J., M. L. Delaney, and J. C. Zachos (2010), Paleoredox changes across the Paleocene-Eocene thermal maximum, Walvis Ridge [ODP Sites 1262, 1263, and 1266]: Evidence from Mn and U enrichment factors, *Paleoceanography*, *25*, PA4202, doi:10.1029/2009PA001861.

Cleveland, C. C., and D. Liptzin (2007), C:N:P stoichiometry in soil: Is there a "Redfield" ratio for the microbial biomass?, *Biogeochemistry*, *85*, 235–252.

Cohen, A. S., A. L. Coe, S. M. Harding, and L. Schwark (2004), Osmium isotope evidence for the regulation of atmospheric CO_2 by continental weathering, *Geology*, *32*, 157–160.

Cohen, A. S., A. L. Coe, and D. B. Kemp (2007), The late Palaeocene-early Eocene and Toarcian [early Jurassic] carbon isotope excursions: A comparison of their time scales, associated environmental changes, causes and consequences, *J. Geol. Soc. London*, *164*, 1093–1108.

Colisimo, A. B., T. J. Bralower, and J. C. Zachos (2006), Evidence for lysocline shoaling at the Paleocene/Eocene thermal maximum on Shatsky Rise, northwest Pacific, in *Proceedings of the Ocean Drilling Program, Sci. Res.*, vol. 198 [online], edited by T. J. Bralower, I. P. Silva, and M. J. Malone, pp. 1–36. [Available at http://www-odp.tamu.edu/publications/198_SR/112/112.htm.]

Colombo, J. C., E. Pelletier, C. Brochu, and M. Khall (1989), Determination of hydrocarbon sources using n-alkane and polyaromatic hydrocarbon distribution indexes. Case study: Rio de le Plata estuary, Argentina, *Environ. Sci. Technol.*, *23*, 888–894.

Cope, J. T., and A. Winguth (2011), On the sensitivity of ocean circulation to arctic freshwater input during the Paleocene/Eocene Thermal Maximum, *Palaeogeogr. Palaeoclimatol. Palaeoecol.*, *306*, 82–94.

Crouch, E. M., G. R. Dickens, H. Brinkhuis, M.-P. Aubry, C. J. Hollis, K. M. Rogers, and H. Visscher (2003), The *Apectodinium* acme and terrestrial discharge during the Paleocene-Eocene thermal maximum: Nannoplankton observations at Tawanui, New Zealand, *Palaeogeogr. Palaeoclimatol. Palaeoecol.*, *194*, 387–403.

Crusius, J., S. Calvert, T. Pedersen, and D. Sage (1996), Rhenium and molybdenum enrichments in sediments as indicators of oxic, suboxic and sulphidic conditions of deposition, *Earth Planet. Sci. Lett.*, *145*, 65–78.

Crusius, J., T. F. Pederson, S. E. Calvert, G. L. Cowie, and O. Tadamichi (1999), A 36 kyr geochemical record of organic matter flux variations and changes in intermediate water oxygen concentrations, *Paleoceanography*, *14*, 248–259.

Davelaar, D. (1993), Ecological significance of bacterial polyphosphate metabolism in sediments, *Hydrobiologia*, *253*, 179–192.

Dickens, G. R. (2011), Down the rabbit hole: towards appropriate discussion of methane release from gas hydrate systems during the Paleocene-Eocene thermal maximum and other past hyperthermal events, *Clim. Past*, *7*, 831–846.

Dickens, G. R., J. R. O'Neil, D. K. Rea, and R. M. Owen (1995), Dissociation of oceanic methane hydrate as a cause of the carbon isotope excursion at the end of the Paleocene, *Paleoceanography*, *10*, 965–971.

Dickson, A. J., A. S. Cohen, and A. L. Coe (2012), Seawater oxygenation during the Paleocene Eocene Thermal Maximum, *Geology*, *40*, doi:10.1130/G32977.1.

Dupuis, C., M.-P. Aubry, E. Steurbaut, W. A. Berggren, K. Ouda, R. Magioncalda, B. S. Cramer, D. V. Kent, R. P. Speijer, and C. Heilmann-Clausen (2003), The Dababiya Quarry section: Lithostratigraphy, clay mineralogy, geochemistry and palaeontology, *Micropaleontology*, *49*, 41–59.

Duursma, E. K., and M. P. R. M. Boisson (1994), Global oceanic and atmospheric oxygen stability considered in relation to the carbon cycle and to different time scales, *Oceanologica Acta.*, *17*, 117–141.

Emerson, S. R., and S. S. Huested (1991), Ocean anoxia and the concentrations of molybdenum and vanadium in seawater, *Mar. Chem.*, *34*, 177–196.

Eriksson, B. E., and G. R. Helz (2000), Molybdenum [IV] speciation in sulphidic waters: Stability and lability of thiomolybdates, *Geochim. Cosmochim. Acta*, *64*, 1149–1158.

Francois, R., S. Honjo, S. J. Manganini, and G. E. Ravizza (1995), Biogenic barium fluxes to the deep sea: Implications for paleoproductivity reconstruction, *Global Biogeochem. Cycles*, *9*, 289–303, doi:10.1029/95GB00021.

Friedrich, O. (2010), Benthic foraminifera and their role to decipher paleoenvironment during mid-Cretaceous Oceanic Anoxic Events—The "anoxic benthic foraminifera" paradox, *Rev. Micropaleontol.*, *53*, 175–192.

©2014. American Geophysical Union. All Rights Reserved.

Friedrich, O., J. Erbacher, and J. Mutterlose (2006), Paleoenvironmental change across the Cenomanian/Turonian Boundary Event [Oceanic Anoxic Event 2] as indicated by benthic foraminifera from the Demerara Rise [ODP Leg 207], *Rev. Micropaleontol.*, *49*, 121–139.

Gavrilov, Y. O., and N. G. Muzylöv (1992), The geochemistry of sapropelite interbeds in the Paleogene of Central Caucasus, *Lithol. Min. Resour.*, *26*, 548–559.

Gavrilov, Y. O., L. A. Kodina, I. Y. Lubchenko, and N. G. Muzylev (1997), The late Paleocene anoxic event in epicontinental seas of Peri-Tethys and formation of the sapropelite unit: Sedimentology and geochemistry, *Lithol. Min. Resour.*, *32*, 427–450.

Gavrilov, Y. O., E. A. Shcherbinina, and N. G. Muzylöv (2000), A Paleogene sequence in central North Caucasus: A response to paleoenvironmental changes, *GFF*, *122*, 51–53.

Gavrilov, Y. O., E. A. Shcherbinina, and H. Oberhänsli (2003), Paleocene-Eocene boundary events in the northeastern Peri-Tethys, in *Causes and Consequences of Globally Warm Climates in the Early Palaeogene*, *GSA Special Paper*, vol. 198, edited by S. L. Wing et al., pp. 25–47, Geol. Soc. Am., Boulder, Colo.

Gavrilov, Y., E. Shcherbinina, O. Golovanova, and B. Porovsky (2009), A variety of PETM records in different settings, northeastern Peri-Tethys, in *Climatic and Biotic Events of the Paleogene [CBEP 2009], Extended Abstracts From an International Conference in Wellington, New Zealand*, *GNS Science Miscellaneous Series*, vol. 18, edited by E. M. Crouch, C. P. Strong, and C. J. Hollis, pp. 67–70.

Gavrilov, Y., E. A. Shcherbinina, O. V. Golovanova, and B. G. Porovsky (2013), The late Cenomanian Paleoecological event (OAE 2) in the Eastern Caucasus Basin of Northern Peri-Tethys, *Lithology and Mineral Resources*, *48*, 457–488.

Georgiev, S., et al. (2012), Chemical signals for oxidative weathering predict Re-Os isochroneity in black shales, East Greenland, *Chem. Geol.*, *324–325*, 108–121.

Gibbs, S. J., T. J. Bralower, P. R. Bown, J. C. Zachos, and M. Bybell (2006), Shelf and open ocean calcareous phytoplankton assemblages across the Paleocene-Eocene Thermal Maximum: Implications for global productivity gradients, *Geology*, *34*, 233–236.

Giger, W., C. Schnaffner, and S. G. Wakeham (1980), Aliphatic and olefinic hydrocarbons in recent sediments of Greifensee, Switzerland, *Geochim. Cosmochim. Acta*, *44*, 119–129.

Handley, L., A. O'Halloran, P. N. Pearson, E. Hawkins, C. J. Nicholas, S. Schouten, I. K. McMillan, and R. D. Pancost (2012), Changes in the hydrological cycle in tropical East Africa during the Paleocene-Eocene Thermal Maximum, *Palaeogeogr. Palaeoclimatol. Palaeoecol.*, *329–330*, 10–21.

Harding, I. C., et al. (2011), Sea-level and salinity fluctuations during the Paleocene-Eocene thermal maximum in Arctic Spitsbergen, *Earth Planet. Sci. Lett.*, *303*, 97–107.

Helz, G. R., E. Bura-Nakić, N. Mikac, and I. Ciglenečki (2011), New model for molybdenum behaviour in euxinic waters, *Chem. Geol.*, *284*, 323–332.

Higgs, N. C., J. Thomson, T. R. S. Wilson, and I. W. Croudace (1994), Modification and complete removal of eastern Mediterranean sapropels by postdepositional oxidation, *Geology*, *22*, 423–426.

Hollis, C. J., G. R. Dickens, B. D. Field, C. M. Jones, and C. P. Strong (2005), The Paleocene-Eocene transition at Mead Stream, New Zealand: A southern Pacific record of early Cenozoic global change, *Palaeogeogr. Palaeoclimatol. Palaeoecol.*, *215*, 313–343.

Huber, M., and L. C. Sloan (2001), Heat transport, deep waters, and thermal gradients: Coupled simulation of an Eocene Greenhouse Climate, *Geophys. Res. Lett.*, *28*, 3481–3484, doi:10.1029/2001GL012943.

Jenkyns, H. C. (2003), Evidence for rapid climate change in the Mesozoic-Palaeogene greenhouse world, *Philos. Trans. R. Soc. London, Ser. A*, *361*, 1885–1916.

Jenkyns, H. C. (2010, Geochemistry of Oceanic Anoxic Events, *Geochem. Geophys. Geosyst.*, *11*, Q03004, doi:10.1029/2009GC002788.

Jimenez Berrocoso, A., K. G. MacLeod, E. E. Martin, E. Bourbon, C. Isaza Londono, and C. Basak (2010), Nutrient trap for Late Cretaceous black shales in the tropical North Atlantic, *Geology*, *38*, 1111–1114.

John, C. M., S. M. Bohaty, J. C. Zachos, A. Sluijs, S. Gibbs, H. Brinkhuis, and T. J. Bralower (2008), North American continental margin records of the Paleocene-Eocene Thermal Maximum: Implications for global carbon and hydrological cycling, *Paleoceanography*, *23*, PA2217, doi:10.1029/2007PA001465.

Kaiho, K., K. Takeda, M. R. Petrizzo, and J. C. Zachos (2006), Anomalous shifts in tropical Pacific planktonic and benthic foraminiferal test size during the Paleocene-Eocene Thermal Maximum, *Palaeogeogr. Palaeoclimatol. Palaeoecol.*, *237*, 456–464.

Keeling, R. F., A. Körtzinger, and N. Gruber (2010), Ocean deoxygenation in a warming world, *Annu. Rev. Mar. Sci.*, *2*, 199–229.

Khozyem, H., T. Adatte, J. E. Spangenberg, A. A. Tantawy, and G. Keller (2013), Palaeoenvironmental and climatic changes during the Palaeocene-Eocene Thermal Maximum (PETM) at the Wadi Nukhul section, Sinai, Egypt, *J. Geol. Soc.*, *170*, 341–352.

Knox, R. W. O.' B., M.-P. Aubry, W. A. Berggren, C. Dupuis, K. Ouda, R. Magioncalda, and M. Soliman (2003), The Qreiya section at Gebel Abu Had: Lithostratigraphy, clay mineralogy, geochemistry and biostratigraphy, *Micropaleontology*, *49*, 93–104.

Kodina, L. A., Y. Huang, Y. O. Gavrilov, M. Jones, and G. Eglinton (1995), Environment of upper Paleocene black shale deposition in Southern Russia and adjacent regions as revealed by isotope and biomarker study, in *Organic Geochemistry: Developments and Applications to Energy, Climate, Environment and Human History: Selected Papers from the 17th International Meeting on Organic Geochemistry*, *Special Papers*, vol. 369, edited by J. O. Grimalt and C. Dorrosoro, pp. 194–192, Geol. Soc. Am., Denostia-San Sebastian, The Basque Country.

Kuypers, M. M. M., R. D. Pancost, I. A. Nijenhuis, and J. S. Sinninghe Damste (2002), Enhanced productivity led to increased organic carbon burial in the euxinic North Atlantic basin during the late Cenomanian oceanic anoxic event, *Paleoceanography*, *17*(4), 1051, doi:10.1029/2000PA000569.

Lippert, P. C., and J. C. Zachos (2007), A biogenic origin for anomalous fine-grained magnetic material at the Paleocene-Eocene boundary at Wilson Lake, New Jersey, *Paleoceanography*, *22*, PA4104, doi:10.1029/2007PA001471.

Lyons, T. W., and S. Severmann (2006), A critical look at iron paleoredox proxies: New insights from modern euxinic marine basins, *Geochim. Cosmochim. Acta*, *70*, 5698–5722.

Lytle, J. S., T. F. Lytle, J. N. Gearing, and P. J. Gearing (1979), Hydrocarbons in benthic algae from the Eastern Gulf of Mexico, *Mar. Biol.*, *51*, 279–288.

Mangini, A., M. Jung, and S. Laukenmann (2001), What do we learn from peaks of uranium and of manganese in deep sea sediments?, *Mar. Geol.*, *177*, 63–78.

März, C., S. W. Poulton, B. Beckmann, K. Kuester, T. Wagner, and S. Kasten (2008), Redox sensitivity of P cycling during marine black shale formation: Dynamics of sulfidic and anoxic, non-sulfidic bottom waters, *Geochim. Cosmochim. Acta*, *72*, 3703–3717.

McInerney, F. A., and S. L. Wing (2011), The Paleocene-Eocene Thermal Maximum: A perturbation of carbon cycle, climate and biosphere with implications for the future, *Annu. Rev. Earth Planet. Sci.*, *39*, 489–516.

Monterio, F. M., R. D. Pancost, A. Ridgwell, and Y. Donnadieu (2012), Nutrients as the dominant control on the spread of anoxia and euxinia across the Cenomanian-Turonian oceanic anoxic event [OAE2]: Model-data comparison, *Paleoceanography*, *27*, PA4209, doi:10.1029/2012PA002351.

Morford, J. L., and S. Emerson (1999), The geochemistry of redox sensitive trace metals in sediments, *Geochim. Cosmochim. Acta*, *63*, 1735–1750.

Mort, H. P., T. Adatte, K. B. Föllmi, G. Keller, P. Steinmann, V. Matera, Z. Berner, and D. Stüben (2007), Phosphorous and the roles of productivity and nutrient recycling during Oceanic Anoxic Event 2, *Geology*, *35*, 483–486.

©2014. American Geophysical Union. All Rights Reserved.

Nesbitt, H. W., and G. M. Young (1998), Early Proterozoic climates and plate motions inferred from major element chemistry of lutites, *Nature*, *299*, 715–717.
Nicolo, M. J., G. R. Dickens, C. J. Hollis, and J. C. Zachos (2008), Multiple early Eocene hyperthermals: Their sedimentary expression on the New Zealand continental margin and in the deep sea, *Geology*, *35*, 699–702.
Nicolo, M. J., G. R. Dickens, and C. J. Hollis (2010), South Pacific intermediate water oxygen depletion at the onset of the Paleocene-Eocene thermal maximum as depicted in New Zealand margin settings, *Paleoceanography*, *225*, PA4210, doi:10.1029/2009PA001904.
O'Connell, S., M. A. Chandler, and R. Ruedy (1996), Implications for the creation of warm saline deep water: Late Paleocene reconstructions and global climate model simulations, *Geol. Soc. Am. Bull.*, *108*, 270–284.
Pagani, M., N. Pedentchouk, M. Huber, A. Sluijs, S. Schouten, H. Brinkhuis, J. S. Sinninghe Damste, G. R. Dickens, and Expedition 302 Scientists (2006), Arctic hydrology during global warming at the Paleocene/Eocene thermal maximum, *Nature*, *442*, 671–675.
Pak, D. K., and K. G. Miller (1992), Paleocene to Eocene benthic foraminiferal isotopes and assemblages: Implications for deepwater circulation, *Paleoceanography*, *7*, 405–422, doi:10.1029/92PA01234.
Pancost, R. D., N. Crawford, S. Magness, A. Turner, H. C. Jenkyns, and J. R. Maxwell (2004), Further evidence for the development of photic-zone euxinic conditions during Mesozoic Oceanic Anoxic Events, *J. Geol. Soc. London*, *161*, 353–364.
Passier, H. F., H-J. Bosch, I. A. Nijenhuis, L. J. Lourens, M. E. Böttcher, A. Leenders, J. S. Sinninghe Damsté, G. J. de Lange, and J. W. Leeuw (1999), Sulphidic Mediterranean surface waters during Pliocene sapropel formation, *Nature*, *397*, 146–149.
Pearce, C. R., A. S. Cohen, and I. J. Parkinson (2009), Quantitative separation of molybdenum and rhenium from geological materials for isotopic determination by MC-ICP-MS, *Geostand. Geoanal. Res.*, *33*, 219–229.
Peucker-Ehrenbrink, B., and R. E. Hannigan (2000), Effects of black shale weathering on the mobility of rhenium and platinum group elements, *Geology*, *28*, 475–478.
Piper, D. Z., and S. E. Calvert (2009), A marine biogeochemical perspective on black shale deposition, *Earth Sci. Rev.*, *95*, 63–96.
Poulton, S. W., and D. E. Canfield (2005), Development of a sequential extraction procedure for iron: Implications for iron partitioning in continentally derived particles, *Chem. Geol.*, *214*, 209–221.
Poulton, S. W., and D. E. Canfield (2011), Ferruginous conditions: A dominant feature of the ocean through Earth's history, *Elements*, *7*, 107–112.
Pruysers, P. A., G. J. De Lange, J. J. Middelburg, and D. J. Hydes (1993), The diagenetic formation of metal-rich layers in sapropel-containing sediments in the eastern Mediterranean, *Geochim. Cosmochim. Acta*, *57*, 527–536.
Radionova, E. P., G. N. Aleksandrova, T. T. Gavtadze, S. I. Stupin, and I. E. Khokhlova (2009), Analysis of late Paleocene-early Eocene microplankton from the Kheu River section, west pre-Caucasus, in *Climatic and Biotic Events of the Paleogene [CBEP 2009]: Extended Abstracts From an International Conference in Wellington, New Zealand, GNS Science Misc. Series*, vol. 18, edited by E. M. Crouch, C. P. Strong, and C. J. Hollis, pp. 111–116.
Raiswell, R., and D. E. Canfield (1998), Sources of iron for pyrite formation in marine sediments, *Am. J. Sci.*, *298*, 219–245.
Ravizza, G., R. N. Norris, J. Blusztajn, and M.-P. Aubry (2001), An osmium isotope excursion associated with the late Paleocene thermal maximum: Evidence of intensified chemical weathering, *Paleoceanography*, *16*, 155–163, doi:10.1029/2000PA000541.
Reitz, A., M. Wille, T. F. Nägler, and G. J. de Lange (2007), Atypical Mo isotope signatures in eastern Mediterranean sediments, *Chem. Geol.*, *245*, 1–8.
Rieley, G., R. J. Collier, D. M. Jones, G. Eglinton, P. A. Eakin, and A. E. Fallick (1991), Sources of sedimentary lipids deduced from stable carbon-isotope analyses of individual compounds, *Nature*, *352*, 425–427.
Roberts, C. D., A. N. LeGrande, and A. K. Tripati (2009), Climate sensitivity to Arctic seaway restriction during the early Paleogene, *Earth Planet. Sci. Lett.*, *286*, 576–585.
Rowland, S. J. (1990), Production of acyclic isoprenoid hydrocarbons by laboratory maturation of methanogenic bacteria, *Org. Geochem.*, *15*, 9–16.
Rudnick, R. L., and S. Gao (2003), Composition of the continental crust, in *Treatise on Geochemistry*, vol. 3, edited by D. H. Heinrich and K. T. Karl, pp. 1–64, Elsevier, Pergamon, Oxford, U. K.
Sannigrahi, P., and E. Ingall (2005), Polyphosphates as a source of enhanced P fluxes in marine sediments overlain by anoxic waters: Evidence from 31P NMR, *Geochem. Trans.*, *6*, 52–59.
Scalan, E. S., and J. E. Smith (1970), An improved measure of the odd-even predominance in the normal alkanes of sediment extracts and petroleum, *Geochim. Cosmochim. Acta*, *34*(5), 611–620.
Schmitz, B., and V. Pujalte (2007), Abrupt increase in seasonal extreme precipitation at the Paleocene-Eocene boundary, *Geology*, *35*, 215–218.
Schmitz, B., R. P. Speijer, and M.-P. Aubry (1996), Latest Paleocene benthic extinction event on the southern Tethyan shelf [Egypt]: Foraminiferal stable isotopic [$\delta^{13}C$, $\delta^{18}O$] records, *Geology*, *24*, 347–350.
Schmitz, B., S. D. Charisi, E. I. Thompson, and R. P. Speijer (1997), Barium, SiO2 (excess), and P2O5 as proxies of biological productivity in the Middle East during the Palaeocene and the latest Palaeocene benthic extinction event, *Terra Nova*, *9*, 95–99.
Schmitz, B., B. Peucker-Ehrenbrink, C. Heilmann-Clausen, G. Åberg, F. Asaro, and C.-T. A. Lee (2004), Basaltic explosive volcanism, but no comet impact, at the Paleocene-Eocene boundary: High-resolution chemical and isotopic records from Egypt, Spain and Denmark, *Earth Planet. Sci. Lett.*, *225*, 1–17.
Schulte, S., F. Rostek, E. Bard, J. Rullktter, and O. Marchal (1999), Variations of oxygen-minimum and primary productivity recorded in sediments of the Arabian Sea, *Earth Planet. Sci. Lett.*, *173*, 205–221.
Schulte, P., C. Scheibner, and R. P. Speijer (2011), Fluvial discharge and sea-level changes controlling black shale deposition during the Paleocene-Eocene Thermal Maximum in the Dababiya Quarry section, Egypt, *Chem. Geol.*, *285*, 167–183.
Scott, C., and T. W. Lyons (2012), Contrasting molybdenum cycling and isotopic properties in euxinic versus non-euxinic sediments and sedimentary rocks: Refining the paleoproxies, *Chem. Geol.*, *324–325*, 19–27.
Seto, K. (1995), Carbon and oxygen isotopic paleoceanography of the Indian and South Atlantic Oceans: Paleoclimate and paleo-ocean circulation, *J. Sci. Hiroshima Univ.*, *10*, 393–485.
Sinninghe Damste, J. S., M. M. M. Kuypers, S. Schouten, S. Schulte, and J. Rullkötter (2003), The lycopaneC31 n-alkane ratio as a proxy to assess palaeoxicity during sediment deposition, *Earth Planet. Sci. Lett.*, *209*, 215–226.
Slomp, C. P., and P. van Cappellen (2007), The global marine phosphorous cycle: Sensitivity to oceanic circulation, *Biogeosciences*, *4*, 155–171.
Slomp, C. P., J. Thomson, and G. J. De Lange (2002), Enhanced regeneration of phosphorous during formation of the most recent eastern Mediterranean sapropel, *Geochim. Cosmochim. Acta*, *66*, 171–1184.
Sluijs, A., and H. Brinkhuis (2009), A dynamic climate and ecosystem state during the Paleocene-Eocene Thermal Maximum: Inferences from dinoflagellate cyst assemblages on the New Jersey shelf, *Biogeosciences*, *6*, 1755–1781.
Sluijs, A., et al. (2006), Subtropical Arctic Ocean temperatures during the Paleocene/Eocene Thermal Maximum, *Nature*, *441*, 610–613.
Sluijs, A., L. van Roij, G. J. Harrington, S. Schouten, J. A. Sessa, L. J. LeVay, G.-J. Reichart, and C. P. Slomp (2013), Extreme warming, photic zone euxinia and sea level rise during the Paleocene/Eocene Thermal Maximum on the Gulf of Mexico coastal plain; connecting marginal marine biotic signals, nutrient cycling and ocean deoxygenation, *Clim. Past Discuss.*, *9*, 6459–6494.

©2014. American Geophysical Union. All Rights Reserved.

Sluijs, A., et al. (2008), Eustatic variations in the Paleocene-Eocene greenhouse world, *Paleoceanography*, *23*, PA4216, doi:10.1029/2008PA001615.
Soliman, M. F. (2003), Chemostratigraphy of the Paleocene/Eocene [P/E] boundary sediments at Gabal el-Qreiya, Egypt, *Micropaleontology*, *49*, 123–138.
Soliman, M. F., M.-P. Aubry, B. Schmitz, and R. M. Sherrell (2011), Enhanced coastal productivity and nutrient supply in upper Egypt during the Paleocene/Eocene Thermla Maximum [PETM]: Mineralogical and geochemical evidence, *Palaeogeogr. Palaeoclimatol. Palaeoecol.*, *310*, 365–377.
Speijer, R. J., and B. Schmitz (1998), A benthic foraminiferal record of Paleocene sea level and trophic/redox conditions at Gebel Aweina, Egypt, *Palaeogeogr. Palaeoclimatol. Palaeoecol.*, *137*, 79–101.
Speijer, R. P., and A. M. Morsi (2002), Ostracode turnover and sea-level changes associated with the Paleocene-Eocene thermal maximum, *Geology*, *30*, 23–26.
Speijer, R. P., and T. Wagner (2002), Sea-level changes and black shales associated with the late Paleocene Thermal Maximum: Organic-geochemical and micropaleontologic evidence from the southern Tethyan margin [Egypt-Israel], in *Catastrophic Events and Mass Extinctions: Impacts and Beyond*, *Special Paper*, vol. 356, edited by C. Koeberl and K. G. MacLead, pp. 533–549, Geol. Soc. Am, Boulder, Colo.
Speijer, R. P., G. J. van der Zwaan, and B. Schmitz (1996), The impact of Paleocene/Eocene boundary events on middle neritic benthic foraminiferal assemblages from Egypt, *Mar. Micropaeontoll.*, *28*, 99–132.
Speijer, R. P., B. Schmitz, and G. J. van der Zwaan (1997), Benthic foraminiferal extinction and repopulation in response to latest Paleocene Tethyan anoxia, *Geology*, *25*, 683–686.
Stassen, P., C. Dupuis, E. Steurbaut, J. Yans, and R. P. Speijer (2012), Perturbation of a Tethyan coastal environment during the Paleocene-Eocene Thermal Maximum in Tunisia [Sidi Nasseur and Wadi Mezzaz], *Palaeogeogr. Palaeoclimatol. Palaeoecol.*, *317–318*, 66–92.
Stein, R., B. Boucsein, and H. Meyer (2006), Anoxia and high primary production in the Paleogene central Arctic Ocean: First detailed records from Lomonosov Ridge, *Geophys. Res. Lett.*, *33*, L18606, doi:10.1029/2006GL026776.
Stupin, S. I., and N. G. Muzylöv (2001), Late Paleocene ecological crisis in the epicontinental basins of the eastern Peri-Tethys: Microbiota and accumulation conditions of sapropelic bed, *Stratigr. Geol. Correl.*, *9*, 501–507.
Thomas, E. (1998), Biogeography of the Late Paleocene benthic foraminiferal extinction, in *Late Paleocene-Early Eocene Climatic and Biotic Events in the Marine and Terrestrial Records*, edited by M.-P. Aubry, S. Lucas, and W. A. Berggren, pp. 214–243, Columbia Univ. Press, New York.
Thurow, J., H.-J. Brumsack, J. Rullkötter, R. Littke, and P. Meyers (1992), The Cenomanian-Turonian Boundary event in the Indian Ocean—A key to understand the global picture, *AGU Geophys. Monogr.*, *70*, 253–274.
Tossell, J. A. (2005), Calculating the partitioning of the isotopes of Mo between oxidic and sulfidic species in aqueous solution, *Geochim. Cosmochim. Acta*, *69*, 2981–2993.
Tribovillard, N., T. J. Algeo, T. Lyons, and A. Riboulleau (2006), Trace metals as paleoredox and paleoproductivity proxies: An update, *Chem. Geol.*, *232*, 12–32.
van Bentum, E. C., G.-J. Reichart, and J. S. Sinninghe Damste (2012), Organic matter provenance, palaeoproductivity and bottom water anoxia during the Cenomanian/Turonian oceanic anoxic event in the Newfoundland Basin [Northern proto North Atlantic Ocean], *Org. Geochem.*, *50*, 11–18.
van Cappellen, P., and E. D. Ingall (1994), Benthic phosphorous regeneration, net primary production, and ocean anoxia: A model of the coupled marine biogeochemical cycles of carbon and phosphorous, *Paleoceanography*, *9*, 677–692, doi:10.1029/94PA01455.
Wakeham, S. G., K. H. Freeman, T. K. Pease, and J. M. Hayes (1993), A photoautotrophic source for lycopene in marine sediments, *Geochim. Cosmochim. Acta*, *57*, 159–165.
Weller, P., and R. Stein (2008), Paleogene biomarker records from the central Arctic Ocean [Integrated Ocean Drilling Program Expedition 302]: Organic carbon sources, anoxia, and sea surface temperature, *Paleoceanography*, *23*, PA1S17, doi:10.1029/2007PA001472.
Westerhold, T., U. Röhl, H. K. McCarren, and J. C. Zachos (2009), Latest on the absolute age of the Paleocene-Eocene Thermal Maximum [PETM]: New insights from exact stratigraphic position of key ash layers +19 and −17, *Earth Planet. Sci. Lett.*, *287*, 412–419.
Wijsman, J. W. M., J. J. Middelburg, P. M. J. Herman, M. E. Böttcher, and C. H. R. Heip (2001), Sulfur and iron speciation in surface sediments along the northwestern margin of the Black Sea, *Mar. Chem.*, *74*, 261–278.
Winguth, A., C. Shellito, C. Shields, and C. Winguth (2010), Climate response at the Paleocene-Eocene Thermal Maximum to greenhouse gas forcing: A model study with CCSM3, *J. Clim.*, *23*, 2562–2584.
Young, G. M., and H. W. Nesbitt (1998), Processes controlling the distribution of Ti and Al in weathering profiles, siliciclastic sediments and sedimentary rocks, *J. Sed. Res.*, *A68*, 448–455.
Zachos, J. C., S. M. Bohaty, C. M. John, H. McCarren, D. C. Kelly, and T. Nielsen (2007), The Palaeocene-Eocene carbon isotope excursion: Constraints from individual shell planktonic foraminifer records, *Phil. Trans. R. Soc. A*, *365*, 1829–1842.
Zachos, J. C., G. R. Dickens, and R. E. Zeebe (2008), An early Cenozoic perspective on greenhouse warming and carbon-cycle dynamics, *Nature*, *451*, 279–283.
Zeebe, R. E. (2013), What caused the long duration of the Paleocene-Eocene Thermal Maximum?, *Paleoceanography*, *28*, 440–452, doi:10.1002/palo.20039.
Zeebe, R. E., J. C. Zachos, and G. R. Dickens (2009), Carbon dioxide forcing alone insufficient to explain Palaeocene-Eocene Thermal Maximum warming, *Nat. Geosci.*, *2*, 576–580.

©2014. American Geophysical Union. All Rights Reserved.